















Original Research

Thyroid Hormone Activation Regulates the Crosstalk between Breast Cancer and Mesenchymal Stem Cells

Annarita Nappi¹, Vittoria D'Esposito^{2,3}, Caterina Miro¹, Alessia Parascandolo^{2,3},
Annunziata Gaetana Cicatiello¹, Serena Sagliocchi¹, Lucia Acampora¹,
Sepehr Torabinejad¹, Federica Restolfer¹, Maddalena Raia⁴, Melania Murolo¹,
Emery Di Cicco¹, Pietro Formisano², Monica Dentice^{1,4,*}

¹Department of Clinical Medicine and Surgery, University of Naples “Federico II”, 80131 Naples, Italy

²Department of Translational Medicine, University of Naples “Federico II”, 80131 Naples, Italy

³The Research Unit (URT) of “Genomic of Diabetes”, Institute for Experimental Endocrinology and Oncology “G. Salvatore”, National Research Council (IEOS-CNR), 80131 Naples, Italy

⁴CEINGE – Biotecnologie Avanzate Società consortile a responsabilità limitata (S.c.a.r.l.), 80131 Naples, Italy

*Correspondence: monica.dentice@unina.it (Monica Dentice)

Academic Editor: Jordi Sastre-Serra

Submitted: 12 August 2024 Revised: 28 November 2024 Accepted: 4 December 2024 Published: 20 January 2025

Abstract

Background: Thyroid Hormones (THs) critically impact human cancer. Although endowed with both tumor-promoting and inhibiting effects in different cancer types, excess of THs has been linked to enhanced tumor growth and progression. Breast cancer depends on the interaction between bulk tumor cells and the surrounding microenvironment in which mesenchymal stem cells (MSCs) exert powerful pro-tumorigenic activities. **Methods:** Primary human MSCs from healthy female donors were co-cultured with DIO2 knock out (D2KO) and wild type (WT) MCF7 breast cancer cells to assess cell growth, migration, invasion and the expression of known epithelial-mesenchymal transition (EMT)- and inflammation-related markers. Furthermore, a surgery-free intraductal delivery model, i.e., the Mouse-INtraDuctal (MIND) injection method, was used as a tool for *in vivo* characterization of breast tumor formation and progression. **Results:** In this study, we uncovered a novel role of THs in regulating the tumor-stroma crosstalk. MCF7 cells enhanced the intracellular activation of THs through the TH-activating enzyme, D2, fostering their EMT properties and the dialogue with MSCs. D2 inactivation reduced the invasiveness of MCF7 cells and their responsiveness to the pro-tumorigenic induction via MSCs, both *in vivo* and *in vitro*. **Conclusions:** Thus, we argue that intracellular activation of THs via D2 is a critical requirement for invasive and metastatic conversion of breast cancer cells, advising the blocking of D2 as a potential therapeutic tool for cancer therapy.

Keywords: thyroid hormones; deiodinases; breast cancer; mesenchymal stem cells

1. Introduction

Breast cancer (BRCA) is the most diagnosed non-cutaneous malignancy and ranks second in terms of cancer-related deaths in the global female population typically aged 30–60 years. The high inherent histological and molecular heterogeneity in the BRCA landscapes is a driving principle delineating its etiology and progression and influencing the response to the modern-day therapy treatments [1]. Clinical management strategies of BRCA patients rely on grade, stage, and tumor subtypes, and, from a genetic point of view, strong evidence show that BRCA epidemiology is influenced by different molecular features: [2–5]. Estrogens, stimulating the division and proliferation of normal breast cells, act clearly as catalysts of BRCA, in which an abnormal estrogen stimulation prompts an imbalanced and uncontrolled cell proliferation not only of these cells but also of stromal cells that support cancer development. Based on the estrogen-dependency organ physiology, the mainstay approach for Estrogen Receptor

(ER)⁺-BRCA treatment is represented by Estrogen Deprivation Therapy (EDT) or surgical mastectomy [6]. ER⁺-BRCA management is a challenging task due to the progression of the disease to estrogen independence, which is inevitable due to cancer relapses. As suggested by the significant recurrence of Estrogen-Independent Breast cancer (EI-BRCA), other non-estrogenic factors could also be responsible for the progression of BRCA. Thyroid Hormones (THs), 3,3',5-Triiodo-L-thyronine (T3) and its inactive precursor L-Thyroxine (T4), have been identified as crucial factors in the progression of BRCA, acting non-genomically at physiological concentrations via Thyrointegrin $\alpha v \beta 3$ receptors [7–10]. This, in clinical terms, implicates that T4 may exert an estrogen-like function acting non-genomically on tumor cell proliferation, regardless of estrogen receptor status. Several epidemiologic evidence reported a strict association between alteration in thyroid status and breast cancer occurrence, suggesting that diagnosed hyperthyroid patients have a significantly higher risk of BRCA compared to euthyroid patients, but no associ-



ation with diagnosed hypothyroidism [11]. Regardless of the systemic Thyroid Hormones (THs) levels, specific extrathyroidal mechanisms control the final THs effects: (i) transporters-mediated cell uptake, via the Monocarboxylate Transporters 8 (MCT8) and 10 (MCT10); (ii) THs Receptors (TR)-mediated cellular transduction, via TR α and TR β ; (iii) iodothyronine deiodinases-mediated THs activation/inactivation, via the activating enzymes D1/D2 and inactivating enzyme D3 respectively [12–17].

The breast tumor microenvironment is getting great attention in sustaining tumor progression through the mutual and dynamic communication between breast cancer cells and the surrounding Adipose Tissue (AT), which is an abundant source of Mesenchymal Stromal/Stem Cells (MSCs) [18–21]. Due to their self-renewal and immunomodulatory capabilities, Mammary Adipose Tissue-derived Mesenchymal Stromal/Stem Cells (MAT-MSCs) play multifunctional roles in the stimulation of BRCA progression [22–26].

Our work aimed at addressing the role of the iodothyronine deiodinase 2 (DIO2)-mediated TH activation in the tumor-stroma crosstalk in the context of breast cancer. Our results indicated that increased expression of the DIO2 enzyme in the breast cancer cells potentiates the invasiveness and the Epithelial-to-Mesenchymal Transition (EMT) of breast cancer. Moreover, the MAT-MSCs-dependent pro-tumorigenic effects require the DIO2-mediated TH activation, which in turn exert a pro-tumorigenic and a pro-inflammatory function.

Taken together, our results reveal that Deiodinases-mediated regulation of THs metabolism impacts the BRCA behavior. THs enhance MAT-MSCs activation, sensitizing their cancer promoter and immunomodulatory properties.

2. Methods

2.1 Cell Cultures, Reagents, and Treatment

The noninvasive breast cancer cell line, MCF7 (ER⁺, PR⁺, HER2⁻, Research Resource Identifiers #RRID: CVCL_0031, ATCC Number: HTB-22) were purchased from The Global Bioresource Center | American Type Culture Collection (ATCC, Manassas, VA, USA) and cultured according to the recommended growth conditions. In detail, MCF7 were grown at 37 °C in Dulbecco's Modified Eagle Medium (DMEM, HiMedia Leading BioSciences Company, Mumbai, Maharashtra, India, Catalog number: AL007-500ML) supplemented with Fetal Bovine Serum to a final concentration of 10% (HiMedia Leading BioSciences Company, Mumbai, Maharashtra, India, Catalog number: RM10432), L-Glutamine (Gibco, Thermo Fisher Scientific, Waltham, MA, USA, Catalog number: 25030024) and Penicillin/Streptomycin (Gibco, Thermo Fisher Scientific, Waltham, MA, USA, Catalog number: 15070063) both to a final concentration of 1%, in a humidified atmosphere with 5% CO₂. In all the experiments in which TH was applied to cells, we used a hormonal concentration that resembles the physiological exposure of cells to

the active hormone T3 (30.0 nM T3, in a time-course treatment of 24–48 hours, Sigma-Aldrich St. Louis, MO, USA, Catalog number: T6397). In all the experiments in which type II deiodinase was inhibited, we used a specific D2 inhibitor, 3,3',5'-Triiodo-L-thyronine, commonly known as reverse-T3, rT3 (30.0 nM rT3, in a time-course treatment of 24–48 hours, Cayman Chemical Company, Ann Arbor, MI, USA, Catalog number: Cay17598). The transfection protocol was performed using Lipofectamine-2000 (Invitrogen™, Carlsbad, CA, USA, Catalog number: 11668019), according to the manufacturer's instructions. All experiments carried out in the current study meet all relevant ethical regulations. Furthermore, all cell lines used have been authenticated and validated by (1) morphology check by microscope, (2) identity verification by Short Tandem Repeat (STR) profiling and (3) mycoplasma detection. Cell lines were thus tested negative for mycoplasma contamination.

2.2 DIO2 Targeted Mutagenesis

The generation of the MCF7 CRISPR/Cas9 control and DIO2 knock out (D2KO) clones is reported elsewhere [27]. In brief, D2KO MCF7 cells were obtained following targeted mutagenesis of the *DIO2* gene in MCF7 cells by using the CRISPR/Cas9 technology from Santa Cruz Biotechnology (Dallas, TX, USA) (*DIO2* CRISPR/Cas9 KO Plasmid (h), Catalog number: sc-402262) and control D2WT MCF7 cells were stably transfected with the CRISPR/Cas9 control plasmid (Control CRISPR/Cas9 Plasmid, Catalog number: sc-418922). 72 hours after transfection, the cells were sorted using Fluorescence Activated Cell Sorting (FACS) for Green Fluorescent Protein expression (FACS gating/sorting strategy is reported in **Supplementary Fig. 1a**). To avoid off-target effects, three different single D2KO clones were selected and analyzed by PCR to identify alterations in coding regions (**Supplementary Fig. 1b**). Furthermore, *DIO2* depletion was confirmed by DNA sequencing (**Supplementary Fig. 1c**).

2.3 Liquid Chromatography Tandem Mass Spectrometry (LC-MS-MS) Analysis for Measurements of Intracellular Thyroid Hormones

The intracellular T3 and T4 levels were measured as previously described [28,29]. Briefly, frozen D2KO and wild type (WT) MCF7 cell samples were homogenized on ice in phosphate buffer containing 0.25 M sucrose, 1 mM EDTA, 0.1 M NaPO₄, and 10 mM 1,4-Dithiothreitol (DTT, Sigma-Aldrich St. Louis, MO, USA, Catalog number: D062), and sonicated. Then, 100.0 µg of protein extract was incubated for 1 hour at 37 °C in 0.3 mL PE buffer with 10 mM DTT. Then, 20 nM T4-13C6 (Sigma-Aldrich St. Louis, MO, USA, Catalog number: T-076) was added to the reactions and incubated at 37 °C for 6 hours. Proteins were precipitated in acetonitrile (Sigma-Aldrich St. Louis, MO, USA, Catalog number: AX0156) and supernatant evapo-

rated to dryness at 37 °C in a rotavapor. The dried extract was reconstituted with 30.0 µL of a 95:5 methanol:NH₄-OH solution (Methanol with 0.1% Ammonium Hydroxide, Honeywell Research Chemicals, Germany, Catalog number: LC2183) and centrifuged at 13,000 rpm for 10 minutes. Samples (5.0 µL) were injected on a Raptor Biphenyl (Restek Srl. Milan, Italy, Catalog number: 9309A12) 2.7 µm, 100 mm → 2.1 mm using as Mobile Phase A 0.1% Formic acid in water and as Mobile phase B 0.1% Formic acid in methanol. Calibration curves (1.0 to 40.0 nM) were prepared dissolving pure T4, T3, and T4-13C6 in 95:5 methanol: NH₄-OH solution. The analyte MRMs were for T3-13C6 (658.07 > 612.1 > 514.1); T3 (652.07 > 606.1 > 508.1); T4 (778.0 > 731.9 > 323.9); T4-13C6 (784.1 > 738.04). Measurements were conducted in triplicate.

2.4 Primary Human Mammary Adipose Tissue-Derived Mesenchymal Stromal/Stem Cells (MAT-MSCs) Isolation

In this study, primary MAT-MSCs were extracted from the mammary adipose tissue of healthy females undergoing surgical mammary reduction, free of neoplastic, metabolic or endocrine diseases [Age: 40.7 ± 9.0; Weight (kg): 68.7 ± 9.0; Height (cm): 166.0 ± 11.5; BMI: 24.8 ± 0.2]. Samples were obtained from the Surgery Department of the University Hospital Center “Federico II” of Naples, with patients and the Institution Ethical Committee (Protocol Number 138/16). Written informed consents were collected before surgical procedures. Briefly, 1.0 mg/mL of Dispase (Sigma-Aldrich St. Louis, MO, USA, Catalog number: C2139) was utilized to enzymatically digest the biopsies to isolate MAT-MSCs [30,31]. Digestion solution was mixed and incubated for 1 hour at 37 °C. The reaction was finally stopped by adding the same volume (1% w/v) of High Glucose Dulbecco’s Modified Eagle Medium (DMEM, HiMedia Leading BioSciences Company, Mumbai, Maharashtra, India, cod. AL007) supplemented with 10% Fetal Bovine Serum (FBS, HiMedia Leading BioSciences Company, Mumbai, Maharashtra, India, cod. RM10432), enriched in L-Glutamine (Gibco, Thermo Fisher Scientific, Waltham, MA, USA, cod. 25030024), Penicillin/Streptomycin (Gibco, Thermo Fisher Scientific, Waltham, MA, USA, cod. 15070063), Antibiotic-Antimycotic (Gibco, Thermo Fisher Scientific, Waltham, MA, USA, Catalog number: 15240062), all of them to a final concentration of 1%. The cell pellet was centrifuged at 1200 g × 5 minutes at 16 °C and then resuspended in full DMEM/F-12 cell culture medium (Dulbecco’s Modified Eagle Medium/Nutrient Mixture F-12, Thermo Fisher Scientific, Waltham, MA, USA, Catalog number: 11320033), passed through a 70-µm Cell Strainer (Corning, Fisher Scientific, Hampton, New Hampshire, USA, Catalog number: 431751) to remove the remaining tissue debris and seeded in cell culture flasks at a density of 5000–10,000 cells/cm². Fresh culture medium was added after 2 days post-seeding. Finally, MAT-MSCs were grown

in full DMEM/F-12 cell culture medium at 37 °C and 5% CO₂, and medium was changed every 48–72 hours. All tests were performed on cells from passages 4 to 10, and cells were routinely tested for Mycoplasma. The cells were tested to be Mycoplasma-free.

2.5 Colony Formation Assay

Colony Formation Assay is reported elsewhere [13]. In brief, D2KO and WT MCF7 cells (5.0 × 10³ cells) were seeded in cell culture plates to form colonies. 1 week after plating, cells were washed with Phosphate-Buffered Solution (PBS) and stained with 1% Crystal Violet (Sigma-Aldrich St. Louis, MO, USA, Catalog number: C6158) in 20% ethanol (Carlo Erba Reagents S.r.l., Cornaredo MI, Italy, Catalog number: 4146052) for 30 minutes at room temperature (RT). Colonies were manually counted and imaged using a Leica DMI8 microscope digital camera system and the Leica Application Suite LAS X Imaging Software – Version 3.6.0.20104 2018 (Leica Microsystems GmbH, Wetzlar, Germany). The counted colonies were plotted as a graph of the number of colonies per field.

2.6 Cell-Cycle Analysis

Cell-cycle analysis was performed as previously described [13]. Cell-cycle profile of D2KO and WT MCF7 cells was determined by FACS analysis (FACS Canto2, Becton Dickinson, Rowa, Italy). After cells synchronization, consisting in 24 hours of serum starvation, at least 10,000 cells were firstly fixed in ice-cold 70% ethanol at –20 °C, and then stained for 10 minutes at room temperature with a mixed solution of 5.0 µg/mL Propidium Iodide (PI) (Sigma-Aldrich St. Louis, Missouri (MO), USA, Catalog number: P4864) and 0.25 mg/mL Ribonuclease I (RNase I, 10 U/µL, Thermo Fisher Scientific, Waltham, MA, USA, Catalog number: EN0601). Obtained data were analyzed with the MODFIT Lt 3.0 Software – Version 3.0 (BD Biosciences, Rome, Italy).

2.7 3D-Mammosphere Formation Assay

Multicellular 3D-mammosphere were generated from subconfluent MCF7 cells using Ultra-Low Attachment surface plates. In brief, D2KO and WT MCF7 cells were resuspended in complete DMEM growth medium and plated in an Ultra-Low Attachment Polystyrene 96-well (Corning™-Costar®, Fisher Scientific, Hampton, NH, USA, Catalog number: 7007) at a final concentration of 5 cells/well, with or without MAT-MSCs Conditioned Media (MAT-MSCs CM, ratio 1:1). Mammosphere diameters were quantified after 2, 5 and 7 days after seeding by Software associated to the Leica DMI8 microscope digital camera system and the Leica Application Suite LAS X Imaging Software (Version 5.0.2, Leica Microsystems GmbH, Wetzlar, Germany). DAPI Nucleic Acid staining (4',6-Diamidino-2-Phenylindole, Dihydrochloride, Invitrogen™, Carlsbad, CA, USA, Catalog number: D1306, Staining Condition:

1:1000 DAPI stock solution 2.5 mg/mL, 10 minutes directly in cell culture medium) and Fluorescence Laser-Scanning Microscopy (Leica Microsystems GmbH, Wetzlar, Germany) for *in vivo* imaging were performed on not-fixed 7 days after seeding mammospheres.

2.8 2D-MAT-MSCs/MCF7 Coculture Assay

The bidirectional interaction between MAT-MSCs and MCF-7 cells was analyzed by performing 2D-MAT-MSCs/MCF7 coculture assay, according to the manufacturer's protocol. In detail, MAT-MSCs (2.5×10^4 cells) were seeded in the bottom chamber of a transwell-6 culture system (Corning™-Costar®, Fisher Scientific, Hampton, NH, USA, Catalog number: 353090, Permeable Support for 6-well plate with 0.4 µm Transparent PET Membrane), while D2KO or WT MCF7 cells (3.5×10^4 cells) were plated in the upper chamber. MAT-MSCs and MCF-7 cells were cocultured, each in own cell growth medium, for 72 hours. In parallel, MAT-MSCs and D2KO and WT MCF7 cells were monocultured, each in its own cell growth medium, as control. After 72 hours, Conditioned Media (CM) were collected, and cells were harvested for RNA extraction analysis.

2.9 Transwell Migration Assay

MAT-MSCs and MCF7 migration assays were performed using Transwell migration chambers (Corning™-Costar®, Fisher Scientific, Hampton, NH, USA, Catalog number: 353182, Permeable Support for 12-well plate with 8.0 µm Transparent PET Membrane). In brief, MAT-MSCs or D2KO and WT MCF7 cells (1.0×10^5 cells) were added to the upper chamber of a transwell insert, while the lower chamber, pre-coated for 30 minutes with a thin Matrigel layer (BD Matrigel Matrix, BD Biosciences Discovery Labware, Europe, Catalog number: 356234), was supplemented with 50% Conditioned Medium (CM) collected from MAT-MSCs or either D2KO and WT MCF7 cells. After 5 days of incubation at 37 °C, cells that remained on the top of the filter were scrubbed off, and cells that had migrated to the underside of the filter were fixed and stained with 1% Crystal Violet in 20% ethanol for 30 minutes at room temperature (RT). Migrated cells were manually counted and imaged using a Leica DMI8 microscope digital camera system and the Leica Application Suite LAS X Imaging Software (Version 5.0.2, Leica Microsystems GmbH, Wetzlar, Germany). The counted cells were plotted as a graph of cells migrated per field.

2.10 RNA Extraction and Real-Time PCR

The total amount of messenger RNAs (mRNAs) was extracted using TRIzol reagent (Life Technologies Ltd, Carlsbad, CA, USA, Catalog number: 15596018). Complementary DNAs (cDNAs) were synthesized using SuperScript™ VILO™ MasterMix (Life Technologies Ltd, Carlsbad, CA, USA, cod. 11755-050) starting from 1.0

µg of mRNA, according to the manufacturer's instructions. On CFX Connect Real-Time PCR Detection System (BioRad, Hercules, CA, USA, cod. 1855201), Real-Time PCR was directed using the fluorescent double-stranded DNA-binding dye SYBR Green (BioRad, Hercules, CA, USA, cod. 1708882). All samples were analyzed in technical triplicate and standardized to an endogenous control, Cyclophilin-A (CYPA). The Relative Quantification (RQ) and the expression of each mRNA were determined utilizing the comparative Ct methodology and expressed as N-fold differences in target gene expression [$N^{\text{target}} = 2^{(\Delta C_t \text{ sample} - \Delta C_t \text{ calibrator})}$]. Specific primers for each gene were designed to work under the same cycling conditions [95 °C for 10 minutes >40 cycles at 95 °C for 15 seconds >60 °C for 1 minute], thus generating amplicons of comparable sizes (200–300 bp). Primer combinations were placed whenever possible to span an exon-exon junction and the total RNAs were digested with DNase to avoid genomic DNA contamination. Primer sequences are indicated in the **Supplementary Data 1**.

2.11 Immuno Blotting

To estimate the total protein expression, MCF7 cells were lysed with ice-cold Protein Lysis Buffer [0.5% TRITON X-100; 25.0 mM TRIS-HCl pH 7.4; 300.0 mM NaCl; 1.0 mM CaCl_2], supplemented with sodium fluoride (NaF, Sigma-Aldrich St. Louis, MO, USA, Catalog number: 201154), sodium orthovanadate (Na_3VO_4 , Sigma-Aldrich St. Louis, MO, USA, Catalog number: S6508), β -glycerophosphate (Sigma-Aldrich St. Louis, MO, USA, Catalog number: G5422), Phenyl-Methyl-Sulfonyl-Fluoride (PMSF, Sigma-Aldrich St. Louis, MO, USA, Catalog number: P7626) and Protease Inhibitor Cocktail (Sigma-Aldrich St. Louis, MO, USA, Catalog number: P8340), for 30 minutes on ice from whole cell lysates. Protein concentration was measured by spectrophotometer absorbance using Bio-Rad Protein Assay Dye Reagent (BioRad, Hercules, CA, USA, Catalog number: 5000006). After protein estimation, each sample was admixed with 2× Protein Loading Buffer [150.0 mM TRIS-HCl pH 6.8; 6.0% SDS; 30% glycerol, Bromophenol Blue] and boiled for 7 minutes at 99 °C for denaturation. Finally, cell proteins were separated by 8–10 or 12% SDS-PAGE followed by Western Blot. The membrane was then blocked with 5% Bovine Albumin Serum (BSA, Sigma-Aldrich St. Louis, MO, USA, Catalog number: A9647) in Tris-Buffered Saline (TBS)-0.2% Tween and incubated over-night at 4 °C with the following primary antibodies: anti-Cyclin-D1 (Santa Cruz Biotechnology, Catalog number: sc-246), anti-E-Cadherin (BD Biosciences, Catalog number: 610181), anti-ERK1/2 (K-23) (Santa Cruz Biotechnology, Catalog number: sc-94), anti-phospho-p44/42 MAPK (ERK1/2) (Thr202/Tyr204) (Cell Signaling, Danvers, MA, USA, Catalog number: 4370), anti-N-Cadherin (Elabscience, Catalog number: E-AB-32170),

anti-p21 [Waf1] (Santa Cruz Biotechnology, Catalog number: sc-397), anti-p27 [Kip1] (BD Transduction Laboratories, Catalog number: 610242), anti-p38 MAPK (Cell Signaling, Catalog number: 9212), anti-phospho-p38 MAPK (Thr180/Tyr182) (Cell Signaling, Catalog number: 9211S), anti-Slug (Cell Signaling, Catalog number: 9585S), anti-Snail (Cell Signaling, Catalog number: 3895S), anti-ZEB1 (abcam, Catalog number: ab-155249) and anti-Tubulin (Santa Cruz Biotechnology, Catalog number: sc-5546), this last used as loading control. Detection was established by using peroxidase-conjugated secondary specific antibodies (anti-mouse IgG-HRP, BioRad, Hercules, CA, USA, Catalog number: 1706516 and anti-rabbit IgG-HRP, BioRad, Hercules, CA, USA, Catalog number: 1706515). The signals were detected by chemiluminescence using an ECL kit (Millipore, Burlington, MA, USA, Catalog number: WBKLS0500) on ChemiDoc XRS+ System/Images Lab Software (BioRad, Hercules, CA, USA, Catalog number: 1708265). All Western Blots were run in triplicate and bands were quantified with ImageJ Software (Version 1.8.0, NIH Image, Bethesda, MD, USA). Dilution for each antibody is reported in **Supplementary Data 2**.

2.12 Immunofluorescence Staining on MCF7 Cell-Cultured Coverslips

For immunofluorescence staining of MCF7 cell-cultured coverslips, attached cells were first washed in cold PBS and then fixed with 100% cold buffered formaldehyde solution 4%, pH 6.9 (Sigma-Aldrich St. Louis, MO, USA, Catalog number: 1004968350) on ice for 10 minutes. Cells were then permeabilized with 0.2% Triton X-100 (Sigma-Aldrich St. Louis, MO, USA, Catalog number: T8787) for 15 minutes, washed with PBS and then blocked for 30 minutes with 2% BSA in PBS. Next, cells were incubated over-night at 4 °C with primary anti-E-Cadherin (BD Biosciences, Catalog number: 610181), anti-N-Cadherin (Elabscience, Catalog number: E-AB-32170) and anti-ZEB1 (abcam, Catalog number: ab-155249) antibodies (dilution for each antibody is reported in **Supplementary Data 2**), appropriately diluted into blocking solution. Next day, cells were washed with PBS and then incubated with Alexa Fluor Cross-Adsorbed Secondary Antibody [anti-mouse IgG (H+L) Highly Cross-Adsorbed Secondary Antibody, Alexa Fluor 594, Invitrogen™, Carlsbad, CA, USA, Catalog number: A-21203; anti-Mouse IgG (H+L) Cross-Adsorbed Secondary Antibody, Alexa Fluor 488, Invitrogen™, Carlsbad, CA, USA, Catalog number: A-11001; anti-Rabbit IgG (H+L) Highly Cross-Adsorbed Secondary Antibody, Alexa Fluor 594, Invitrogen™, Carlsbad, CA, USA, Catalog number: A-21207; anti-Rabbit IgG (H+L) Cross-Adsorbed Secondary Antibody, Alexa Fluor 488, Invitrogen™, Carlsbad, CA, USA, Catalog number: A-11070], in the dark, at room temperature (RT), for 1 hour. Finally, after the DAPI Nucleic Acid staining, coverslips were mounted using 80% glycerol. The images were cap-

tured using a Leica DMi8 microscope and the Leica Application Suite LAS X Imaging Software (Version 5.0.2, Leica Microsystems GmbH, Wetzlar, Germany) and quantified using ImageJ Fiji Software (Version 2.14.0, ImageJ Wiki, Madison, WI, USA).

2.13 Multiplex Enzyme-Linked Immunosorbent (ELISA) Assay

D2KO and WT MCF7 cells were normally cultured and 72 hours post-plating Conditioned Media were collected and screened for the concentration of a panel of different cytokines and chemokines (i.e., Interleukin-1 β (IL-1 β), IL-6, IL-8, IL-10, Interleukin-1 Receptor Antagonist (IL-1RA), Interleukin-1 Receptor alpha (IL-6 R alpha), B-Cell Activating Factor (BAFF), Vascular-Endothelial Growth Factor (VEGF), Chemokine C-C motif Ligand-3 (CCL-3), CCL-4, CCL-11, C-X-C motif chemokine ligand 10 (CXCL-10), FURIN, CRIPTO, alpha Synuclein, urokinase (u-PA), Interferon- γ (IFN- γ), Tumor Necrosis Factor-alpha (TNF-alpha) and Total Inhibin) using a custom Human Magnetic Luminex Assay (CUSTOM-LXSA-H-21, R&D System), according to the manufacturer's protocol. The magnetic bead-based multiplex assay was performed on a Luminex® 200™ System (Bio-Techne, R&D Systems, Austin, TX, USA, Catalog number: LX200-XPON-RUO) and the results were analyzed with xPONENT® Software 4.3. Concentration (expressed as pg/mL) of detected molecules are reported in Table 1 and **Supplementary Data 3**.

2.14 Animal Studies and Mouse-INtraDuctal (MIND) Injection

All animal procedures were approved by the Institutional Animal Care and Use Committee (IACUC, nos. 167/2015-PR and 354/2019-PR) and conducted in accordance with the guidelines of the "Department of Human Health, Animal Health and Ecosystem and International Relations" from Ministero della Salute (MSAL). 2-months-old male C57BL/6 mice, purchased from Charles River Laboratories (Wilmington, MA, USA), were intraductally xenografted in absence of any surgical manipulation. In detail, mice were anesthetized by 0.01 mL/g intraperitoneal (IP) injection with ketamine (9.0 mg/mL), and the hair surrounding the the fourth pair of abdominal mammary glands were trimmed with a shaver and wiped with 70% ethanol. 2.0×10^5 D2KO and WT MCF7 cells, suspended in 10.0 μ L of sterile PBS, were backloaded into the Insulin Syringes U-100 30G 1.0 mL/cc 5/16" (8 mm). The needle was gently inserted directly into the mammary duct of mice and tumor cells were slowly ejected. Mammary glands were collected 8 weeks post-tumor cell injection. At the end of the experimental procedures, animals were euthanized by exposure to a mixture of isoflurane and oxygen (4% isoflurane e 0,8 Lt/min oxygen) by inhalation and then killed by cervical dislocation.

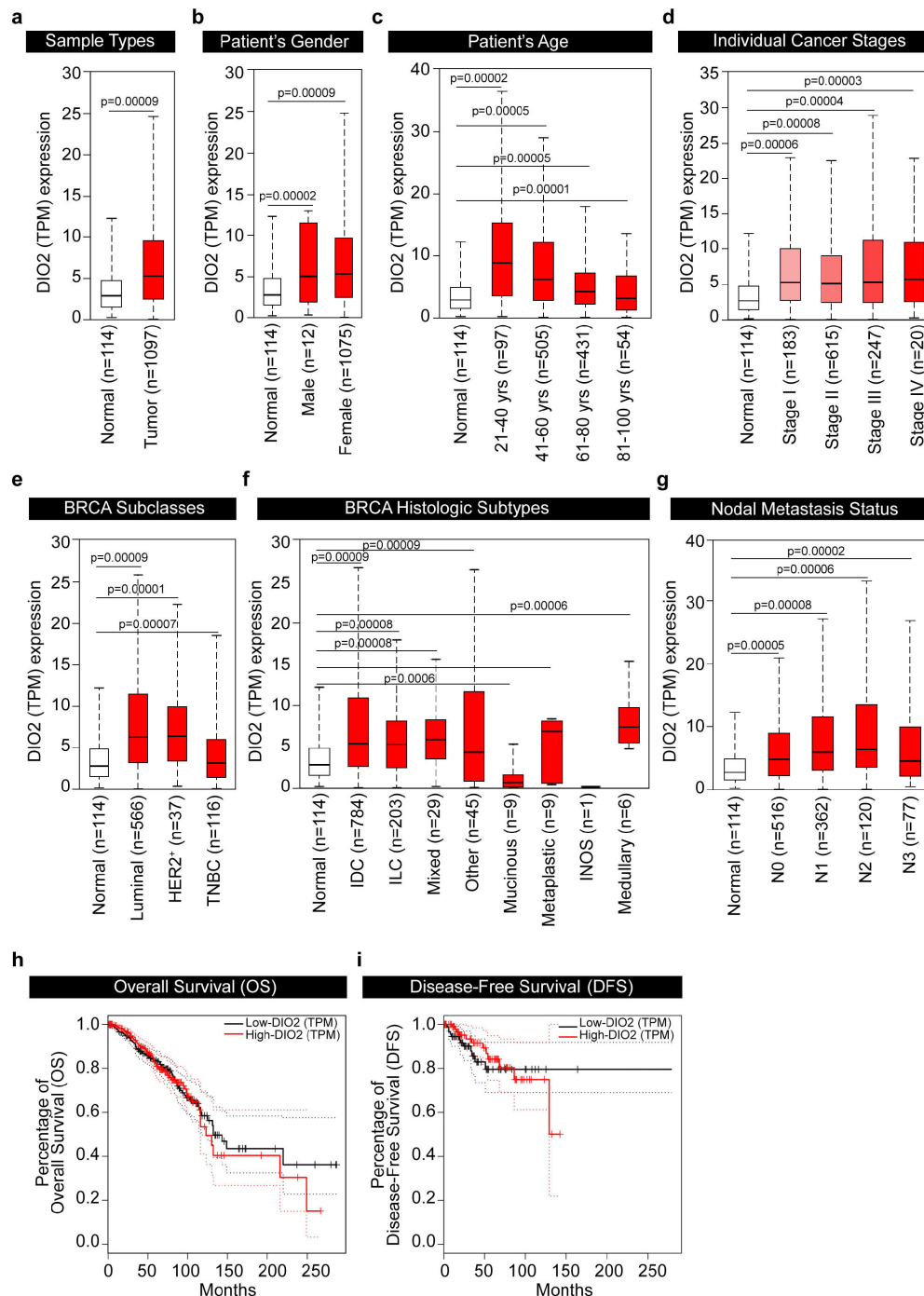


Fig. 1. In-depth the cancer genome atlas program (TCGA) *DIO2* gene expression analyses in BRCA. (a–g) Differential *DIO2* gene expression analysis between normal and BRCA samples (a), stratified in function of patient's gender (b), patient's age (c), individual cancer stages (d), BRCA subclasses (e), BRCA histologic subtypes (f) and nodal metastasis status (g) through the online UALCAN Database (<https://ualcan.path.uab.edu>). *DIO2* levels, expressed as transcripts per million (TPMs), are shown using box plots. (h,i) Kaplan-Meier curves for patient's overall survival (OS) (h) and disease-free survival (DFS) (i) classified by low and high *DIO2* gene expression levels in BRCA (OS and DFS median, hazard ratio (HR) with 95% confidence interval), performed using the survival plot module of GEPIA2 tool (<http://gepia2.cancer-pku.cn>). Statistical analyses were computed by the Wilcoxon test. TPM, transcripts per million; TNBC, triple negative breast cancer; IDC, infiltrating ductal carcinoma; ILC, infiltrating lobular carcinoma; INOS, infiltrating carcinoma NOS; N0-N1-N2-N3 are pathologic_N descriptions in UALCAN. In detail: N0: No regional lymph node metastasis; N1: Metastases in 1 to 3 axillary lymph nodes; N2: Metastases in 4 to 9 axillary lymph nodes; N3: Metastases in 10 or more axillary lymph nodes.

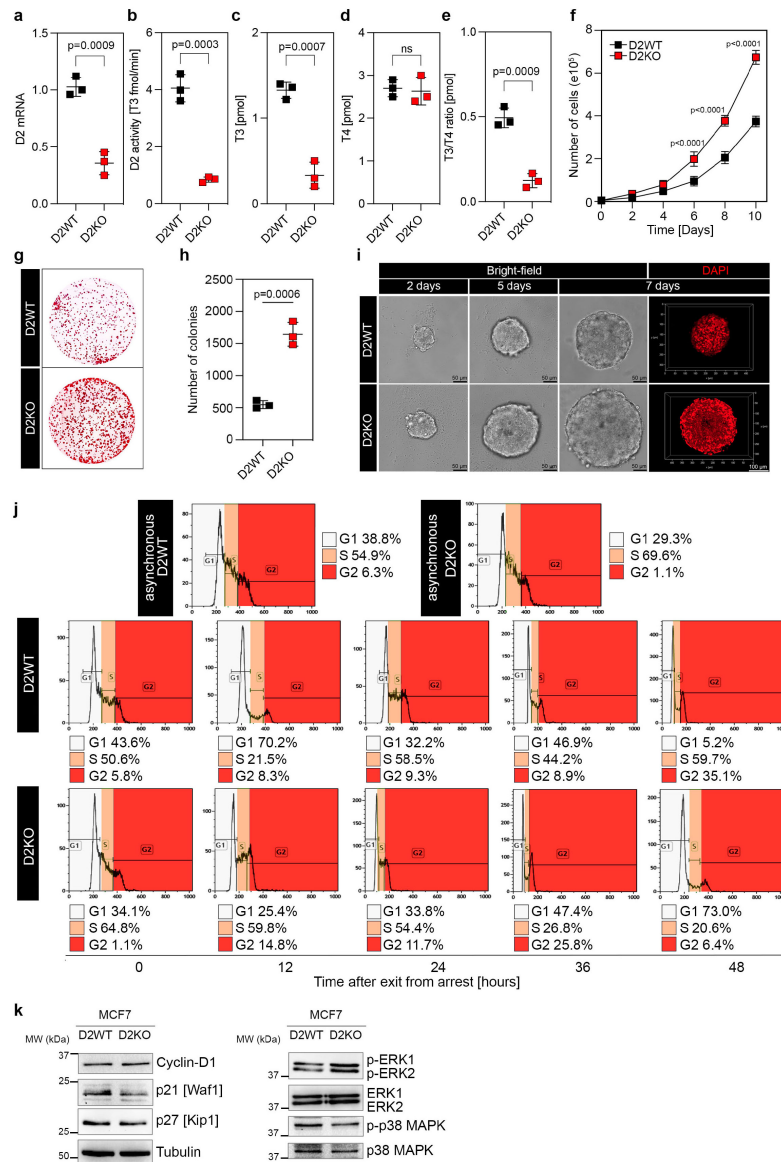


Fig. 2. Lowering of THs intracellular levels through the *DIO2* genetic depletion enhances breast cancer cell proliferation. (a) mRNA expression of D2 assessed by real-time PCR in *DIO2* knock out (D2KO) and wild type (WT) MCF7 cells. (b) D2 deiodinase assay was performed in D2KO and WT MCF7 total protein cells lysates and expressed as amount of heavy T3 produced per hour using heavy T4 as substrate. (c–e) T3 levels [pmol] (c), T4 levels [pmol] (d) and T3/T4 ratio levels [pmol] (e) produced by the deiodination assay performed in D2KO and WT MCF7 total protein cells lysates. (f) Growth curves of D2KO and WT MCF7 cells. (g,h) Clonogenicity of D2KO and WT MCF7 cells determined by colony formation assay by seeding cells (5.0×10^3 cells per well in 6-well plates) and growing for 1 week. Magnification $4\times$. (i) Clonogenicity of D2KO and WT MCF7 cells determined by 3D-Mammosphere Formation Assay. Scale bars represent 50 μm . Quantification of the relative sphere diameters are shown in **Supplementary Fig. 3a**. (j) Flow cytometry cell-cycle distribution in asynchronous and synchronized D2KO and WT MCF7 cells at 0, 12, 24, 36 and 48 hours after exit from arrest. (k) Western blot analysis of cell-cycle and regulatory proteins (Cyclin-D1, p21 [Waf1], p27 [Kip1], p-ERK1/2, p-p38 MAPK) in D2KO and WT MCF7 cells. Tubulin was used as loading control. The immunoblot quantifications (Densitometry Analysis) are shown in **Supplementary Fig. 4a** and the uncutted/unprocessed gels were provided in the **Supplementary Source Data file**. All the results are shown as means \pm SD from at least 3 independent experiments. p -values were determined by the two-tailed Student's t -test. THs, thyroid hormones; mRNA, messenger RNA; D2, type II deiodinase; T3, 3,3',5-Triiodo-L-thyronine; T4, l-thyroxine; ERK, extracellular signal-regulated kinase; MAPK, mitogen-activated protein kinase; PCR, polymerase chain reaction; MW, molecular weight; ns, not significant. Source data are provided as a **Supplementary Source Data file**.

2.15 Hematoxylin/Eosin and Immunostaining of Mouse-INtraDuctal (MIND) Tumors

For histology and immunostaining, engrafted mammary glands were harvested, fixed in 10% neutral buffered formalin (Bio-Optica, Milano, Italy, Catalog number: 05-01005Q) and paraffin-embedded. Hematoxylin/Eosin (H/E) and immunostaining were performed on 15.0 μ m thick tissue sections. Embedded-murine mammary gland sections were dewaxed in xylene, subsequently passed through decreasing ethanol concentrations for rehydration and then permeabilized in 0.2% Triton X-100/PBS. Slides were stained with Hematoxylin Solution (Sigma-Aldrich St. Louis, MO, USA, Catalog number: GHS116) and counterstained with Eosin Y Solution (Sigma-Aldrich St. Louis, MO, USA, Catalog number: HT110216) prior to dehydrating and mounting with Eukitt mounting Solution (BioOptica S.p.A, Milan, Italy, Catalog number: 09-00250). For immunostaining analysis, sections were blocked in 1% Bovine Serum Albumin (BSA, Sigma-Aldrich St. Louis, MO, USA, Catalog number: A9647)/0.2% Tween (Sigma-Aldrich St. Louis, MO, USA, Catalog number: P2287)/PBS for 1 hour at room temperature (RT). Primary antibodies were incubated over-night at 4 °C in the blocking buffer and then washed in 0.2% Tween/PBS. Secondary antibodies were incubated at room temperature (RT) for 1 hour and washed in 0.2% Tween/PBS. Images were acquired with a Leica DMi8 microscope and the Leica Application Suite LAS X Imaging Software.

2.16 Isolation and Analysis of CTCs from Mice Blood Samples

The isolation and Analysis of CTCs from Mice Blood Samples have been reported elsewhere [32]. In brief, mice blood samples were collected in RNA Protect Animal Blood Tube and stored at 4 °C. When necessary, the tubes were incubated at room temperature (RT) for 2 hours to achieve complete lysis of blood cells and total RNA was purified using the RNeasy Protect Animal Blood Kit (QIAGEN, Hilden, Germany, Catalog number: 73224). Complementary DNAs (cDNAs) were synthesized using SuperScript™ VILO™ MasterMix (Invitrogen™, Carlsbad, California (CA), USA, Catalog number: 11755-050) and the samples were tested by Real-Time PCR for the expression of typical clinical biomarkers for breast cancer patients, i.e., Krt8, Krt18, Krt19 and c-Met. For primer sequences see **Supplementary Data 1**.

2.17 Statistics

The data are expressed as means \pm Standard Deviation (SD) of 3 independent experiments. Statistical differences and significance between samples were determined using the Student's two-tailed *t*-test or Ordinary one-way ANOVA. A *p*-value < 0.05 was considered statistically significant. The reproducibility, sample sizes and, where appropriate, statistical analyses are described in the Figure Legends.

3. Results

3.1 Type 2 Deiodinase is Expressed in Breast Cancer and Correlates with Poor Prognosis

To explore the *DIO2* gene expression, prognosis, and clinicopathological characteristics in human breast cancer, we collected data from The Cancer Genome Atlas-BReast Cancer (TCGA-BRCA, <https://portal.gdc.cancer.gov/projects/TCGA-BRCA>) Data Portal and performed a bioinformatic analysis of the differential gene expression in normal and primary breast cancer samples, stratified or not in function of specimens and different histopathological tumor stage. We observed that *DIO2* was significantly overexpressed in BRCA tumor tissues (Fig. 1a) and enhanced independently of patient's gender (Fig. 1b), age (Fig. 1c), individual cancer stage (Fig. 1d), BRCA subclass (Fig. 1e), BRCA histologic subtype (Fig. 1f) and presence and/or absence of nodal metastasis status (Fig. 1g). Additionally, to evaluate the prognostic value of *DIO2* in breast cancer, we carried out Kaplan-Meier analysis. By dividing the cancer cases into low- and high-*DIO2* expression groups according to the *DIO2* expression levels, we found that high-*DIO2* expression breast cancer group had lower Overall Survival (OS) (HR = 0.97, Log Rank *p* = 0.86) (Fig. 1h) and Disease-Free Survival (DFS) (HR = 0.79, Log Rank *p* = 0.57) than those with low-*DIO2* levels (Fig. 1i). Conversely, *DIO3* gene expression was significantly downregulated in breast cancer tissues and reduced in each above-mentioned condition (**Supplementary Fig. 2**). These data suggest that the TH modulating enzymes are inversely regulated in breast cancer, advising that TH status might be fine regulated in human breast cancer cells.

3.2 *DIO2* Targeted Depletion Enhances the Proliferation of Breast Cancer Cells

To address the functional relevance of *DIO2* expression in breast cancer, we genetically depleted the *DIO2* gene using CRISPR/Cas9 technology in a noninvasive breast cancer cell line, MCF7. Effective *DIO2* depletion in D2KO cells was verified by measuring D2 mRNA levels and enzymatic activity (Fig. 2a,b). Moreover, the intracellular T3 and T3/T4 ratio was potently reduced in the D2KO versus WT cells, confirming that D2KO cells have a lower availability of T3 consequent to *DIO2* depletion (Fig. 2c–e). We then analyzed the functional consequences of *DIO2* targeted mutagenesis on cell proliferation. A significant enhancement of cell growth was observed after *DIO2* genetic depletion in MCF7 cell line compared to control cells (Fig. 2f). Accordingly, colony formation assay confirmed a growth advantage for the *DIO2*-depleted cells (Fig. 2g,h). Moreover, we found that also the anchorage-independent growth of MCF7 cells was affected after *DIO2* depletion, as shown by the enhanced sphere diameters compared to control cells (Fig. 2i and **Supplementary Fig. 3a**). Analysis of the cell-cycle progression showed that *DIO2*-depletion

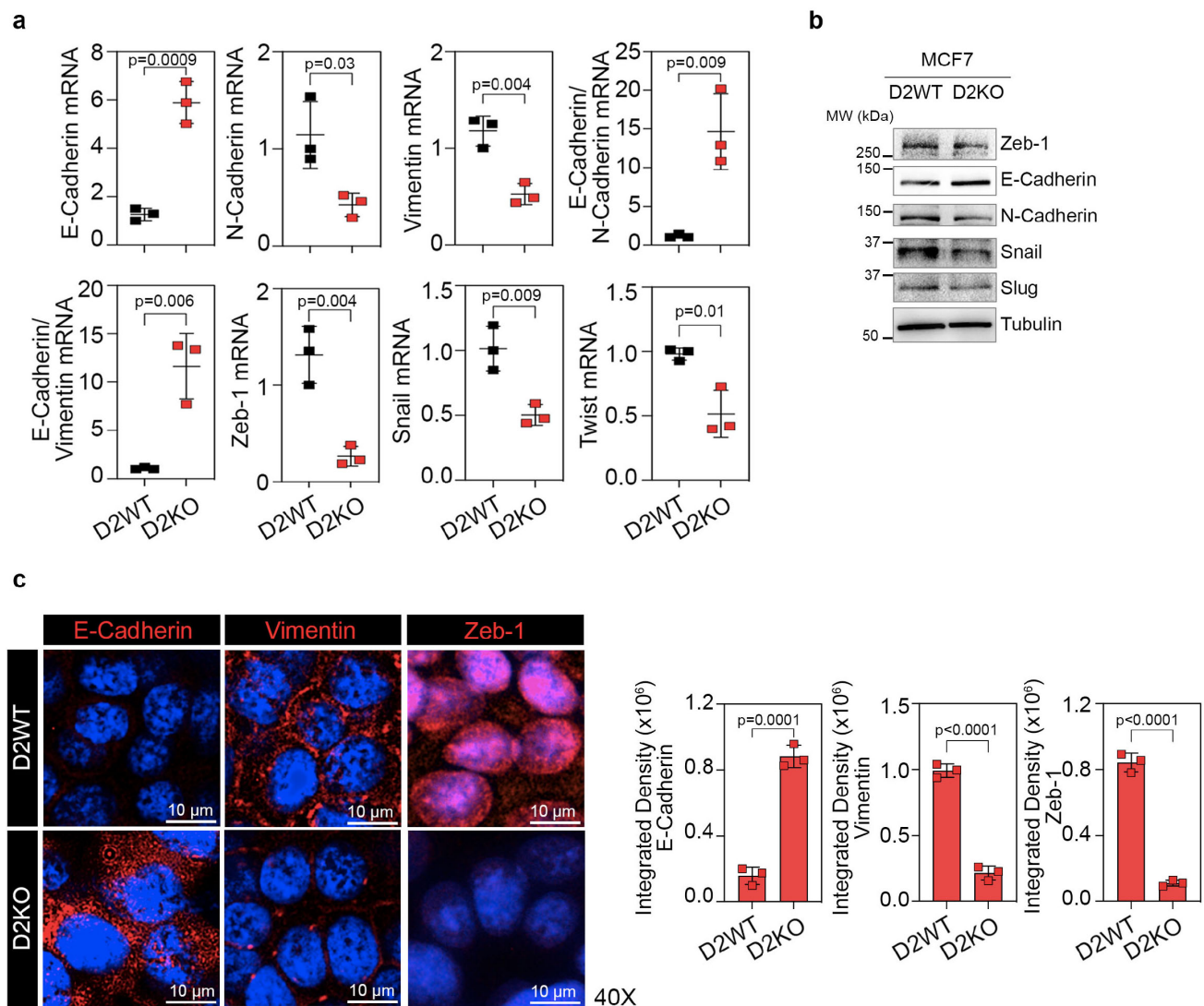


Fig. 3. Loss of D2 attenuates the THs-dependent epithelial-to-mesenchymal transition (EMT) program. (a) mRNA expression of epithelial (E-Cadherin) and mesenchymal (N-Cadherin, Vimentin, Zeb-1, Snail, Twist) markers and their ratio assessed by real-time PCR in DIO2 knock out (D2KO) and wild type (WT) MCF7 cells. (b) Western blot analysis of EMT markers in D2KO and WT MCF7 cells. Tubulin was used as loading control. The immunoblot quantifications (densitometry analysis) are shown in **Supplementary Fig. 5a** and the uncutted/unprocessed gels were provided in the **Supplementary Source Data file**. (c) Confocal images of E-Cadherin, Vimentin and Zeb-1 immunofluorescent staining in D2KO and WT MCF7 cells. Data are presented as higher magnification overviews (representative of 3 images per sample). Magnification 40 \times . Scale bars represent 10 μ m. Relative quantification of E-Cadherin, Vimentin and Zeb-1 immunofluorescent signals (Integrated Density) are represented by histograms. All the results are shown as means \pm SD from at least 3 separate experiments. *p*-values were determined by two-tailed Student's *t*-test. Source data are provided as a **Supplementary Source Data file**.

altered the cell-cycle phase distribution in asynchronous cells, increasing the population of cells in S-phase and reducing those in G1- and G2-phases. In addition, analysis of cell-cycle progression in synchronized cells confirmed that loss of D2 results in a higher percentage of duplicating cells already 12 h after the release from the arrest of the cell cycle compared to control cells (Fig. 2j and **Supplementary Fig. 3b**). To evaluate if enhanced cell proliferation was linked to the reduction of TH signal activa-

tion, we measured the protein expression of known positive (p21 [Waf1], p27 [Kip1]) and negative (Cyclin-D1) TH target genes involved in the control of the cell-cycle [33–35]. Compared to control cells, Cyclin-D1 and phospho-ERK expression was mildly increased in D2KO cells, while the expression of cell-cycle inhibitors p21 [Waf1] and p27 [Kip1] and the anti-proliferative phospho-p38 MAPK was reduced, confirming that *DIO2* depletion also in the BRCA context increases the expression of a negative TH target

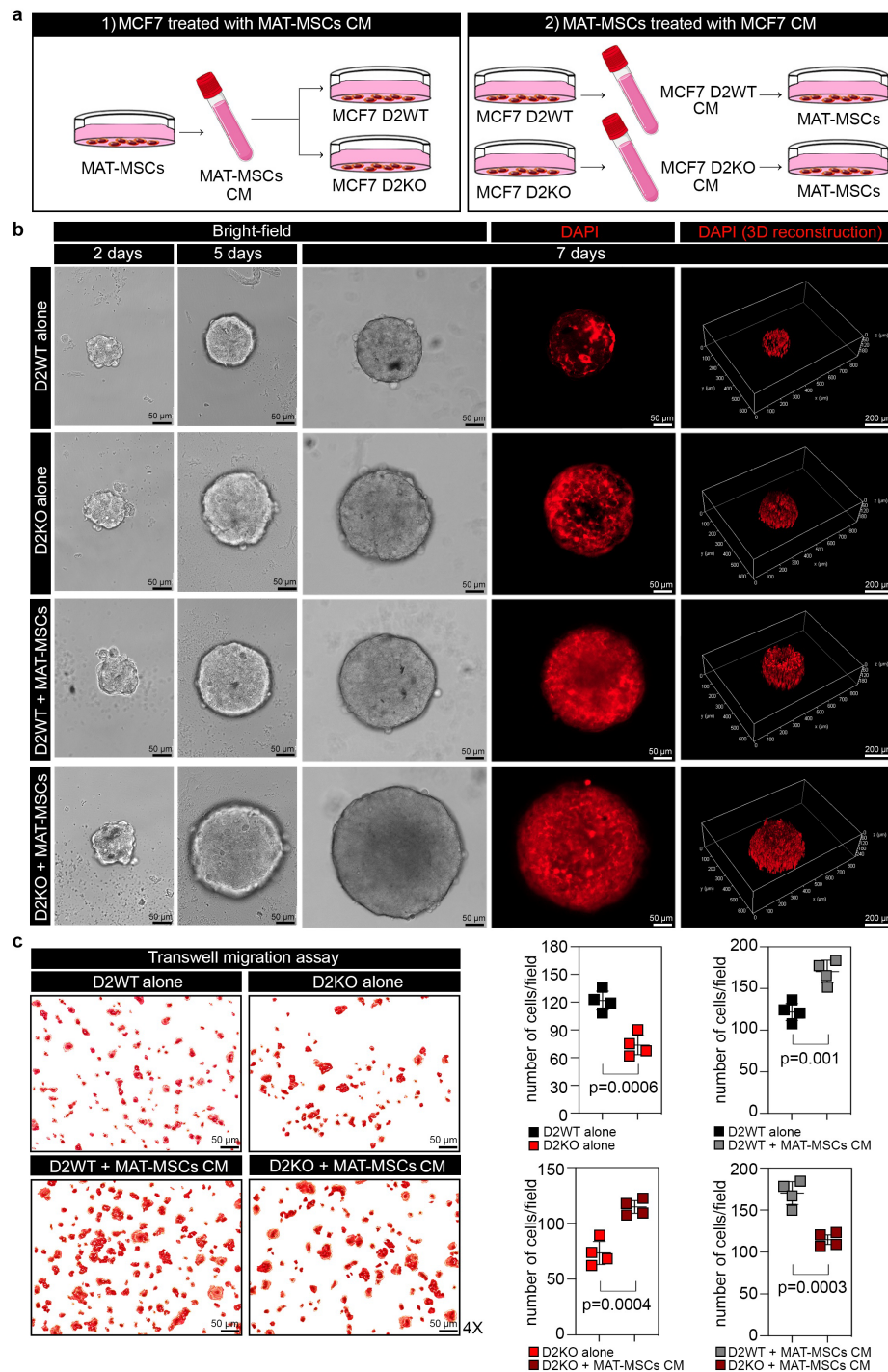


Fig. 4. Attenuation of TH signaling via *DIO2*-depletion impacts on MCF7/MAT-MSCs crosstalk. (a) Schematic illustrating experimental design. Conditioned Media (CM) from (1) MAT-MSCs and (2) D2KO and WT MCF7 cells were collected and used to study their reverse/reciprocal influence in proliferation and migration assays. (b) Clonogenicity of D2KO and WT MCF7 cells, treated or not with MAT-MSCs CM, was determined by 3D-mammosphere formation assay. Quantification of relative sphere diameters is shown in **Supplementary Fig. 7a**. Magnification 10 \times . Scale bars represent 50 or 200 μ m. (c) Migration ability of D2KO and WT MCF7 cells, treated or not with MAT-MSCs CM, was determined by transwell migration assay. Magnification 4 \times . Scale bars represent 50 μ m. The overall motility, expressed as the number of migrated cells/fields, is shown using scatter dot plots. All the results are shown as means \pm SD from at least 3 independent experiments. *p*-values were determined by the two-tailed student's *t*-test. Source data are provided as a **Supplementary Source Data file**.

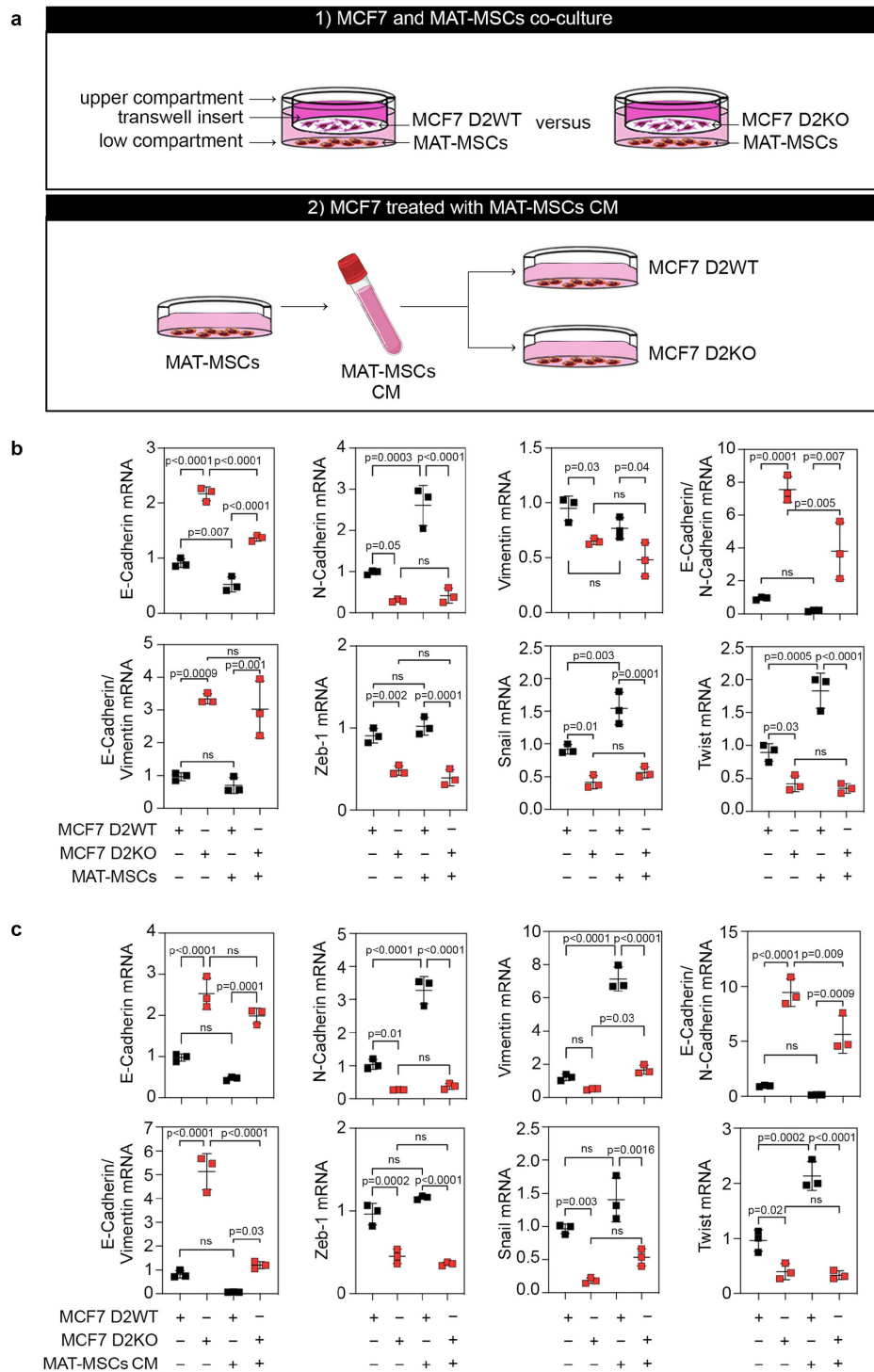


Fig. 5. Thyroid status of MCF7 cells influences their MAT-MSCs-dependent EMT stimulation. (a) Schematic illustrating experimental design. (1) Co-culture experiments of MAT-MSCs and D2KO or WT MCF7 cells; (2) Conditioned media (CM) from MAT-MSCs was collected and used to treat D2KO and WT MCF7 cells. Both experimental conditions have been used to assay MAT-MSCs influence on breast cancer cell EMT properties. (b,c) mRNA expression of epithelial (E-Cadherin) and mesenchymal (N-Cadherin, Vimentin, Zeb-1, Snail, Twist) markers and their ratio assessed by real-time PCR in D2KO and WT MCF7 cells, co-cultured with MAT-MSCs (b) or treated with MAT-MSCs CM (c). All the results are shown as means \pm SD from at least 3 separate experiments. *p*-values were determined by ordinary one-way ANOVA. ns, not significant; MAT-MSCs, mammary adipose tissue-derived mesenchymal stromal/stem cells. Source data are provided as a **Supplementary Source Data file**.

gene, Cyclin-D1, and reduces the expression of positive TH target genes, p21 [Waf1], p27 [Kip1] (Fig. 2k and **Supplementary Fig. 4a**). To further confirm that the D2KO-dependent increase in cell growth was due to the blockage of the D2-mediated T4-to-T3 conversion, we treated D2KO cells with physiological T3 concentrations and observed that T3 treatment rescued the fast-cycling profile of D2KO cells (**Supplementary Fig. 4b**). Analogously, the treatment of MCF7 control cells with a specific D2 inhibitor, reverse-T3 (rT3) [36], enhanced the proliferation rate of D2WT cells to almost that of D2KO cells (**Supplementary Fig. 4c**). These findings indicate that *DIO2* genetic ablation, reducing the nuclear T4-to-T3 conversion, enhances cell proliferation of MCF7 cells by reducing the expression of genes involved in cell-cycle arrest and fostering the expression of proliferative genes.

3.3 Loss of D2 Reduces the TH-Dependent Epithelial-to-Mesenchymal Transition

Given the enhanced *DIO2* expression in human breast cancer progression and the correlation with a poor prognosis in breast cancer patients, we investigated whether the D2-mediated TH activation could be responsible for the invasive conversion of breast cancer cells. Therefore, we evaluated the contribution of the TH signal in promoting the epithelial-to-mesenchymal transition (EMT) in MCF7 breast cancer cells. As shown in Fig. 3a, *DIO2* depletion reduced the expression of known EMT markers (i.e., N-Cadherin, Vimentin, Zeb-1, Snail, Slug, and Twist), in association with a remarkable induction of the epithelial marker E-Cadherin, thereby resulting in a clear attenuation of the E-Cadherin/N-Cadherin ratio and E-Cadherin/Vimentin ratio at mRNA levels. The same results were obtained by analyzing the protein expression of epithelial and mesenchymal markers by Western Blot and immunofluorescence staining (Fig. 3b,c). To verify whether the activation of the TH signal is a mandatory requisite of the EMT induction in breast cancer cells, we treated D2KO cells with T3 in a time-course and observed that TH treatment rescued the loss of mesenchymal phenotype acquired as a consequence of the genetic *DIO2* ablation (**Supplementary Fig. 5**). As an additional control of TH-dependent EMT induction, we treated MCF7 WT cells with rT3 in a time-course and we observed that the expression of mesenchymal markers was reduced, while the expression of the epithelial marker E-Cadherin was enhanced at both mRNA and protein levels (**Supplementary Fig. 6**). Overall, these data demonstrate that the genetic *DIO2* depletion attenuates the breast cancer EMT, lowering the propensity to acquire an invasive phenotype.

3.4 The D2-Mediated TH Activation Influences the MAT-MSCs/MCF7 Crosstalk

To investigate if the D2-mediated TH activation influences the tumor-stroma crosstalk in the breast cancer

context, we cultured the D2KO and WT MCF7 cells with Conditioned Media (CM) from Mammary Adipose Tissue-derived Mesenchymal Stromal/Stem Cells (MAT-MSCs) and, in addition, we studied the reverse influence of D2KO and WT MCF7 cells on MAT-MSCs (Fig. 4a). CM from three different patients-derived MAT-MSCs (MAT-MSCs CM) were collected and used to define the effects of stromal secreted soluble factors on the proliferation and migration of D2KO and WT MCF7 cells. MAT-MSCs CM increased cell proliferation of WT MCF7 cells compared to MCF7 cultured alone as control and this effect was enhanced in D2KO MCF7 cells (Fig. 4b and **Supplementary Fig. 7a,b**). In contrast, the genetic ablation of *DIO2* in MCF7 cells did not change the morphology and the proliferation rate of MAT-MSCs, as indicated by the unaltered cell density (**Supplementary Fig. 7c**). These results indicate that not only the D2-mediated TH activation influences the MCF7 behavior in term of proliferation, but also their responsiveness to the Mesenchymal Stromal/Stem Cells.

Next, we evaluated the migration ability of D2KO and WT MCF7 cells conditioned or not with the growth media of MAT-MSCs. Treatment with MAT-MSCs CM increased the migration ability of MCF7 cells compared to own monoculture cells as control and this effect was appreciably attenuated in D2KO MCF7 cells (MCF7 D2WT alone: 121.8 ± 10.2 ; MCF7 D2KO alone: 73.5 ± 10.3 ; MCF7 D2WT + CM MAT-MSCs: 170.3 ± 13.6 ; MCF7 D2KO + CM MAT-MSCs: 114.8 ± 5.7) (Fig. 4c). When we performed the inverse experiment, i.e. the reciprocal influence of D2KO and WT MCF7 CM on the migration of MAT-MSCs, we observed that the migration of MAT-MSCs was enhanced by the CM of both D2KO and WT MCF7 cells compared to MAT-MSCs alone, with no differences between CM of D2KO and WT MCF7 cells (**Supplementary Fig. 7d**).

Then, we evaluated the EMT transcriptomic signature from D2KO and WT MCF7 cocultured or conditioned with the medium of MAT-MSCs versus matched D2KO and WT MCF7 monocultured as control (Fig. 5a). Similar to what was observed in D2KO and WT MCF7 comparison (Fig. 3), mRNA expression profile of EMT genes in the MCF7 cocultured with MAT-MSCs indicated that MAT-MSCs enhanced the overall MCF7 cell EMT propriety in dependence of the thyroid status of breast cancer cells. In detail, the expression of the epithelial marker E-Cadherin in D2KO and WT MCF7 cells cocultured with MAT-MSCs was reduced compared to their corresponding monocultured control group, and concurrently the expression of mesenchymal markers N-Cadherin and Vimentin and EMT-associated transcription factors, including Zeb-1, Snail and Twist, had the opposite trend (Fig. 5b). Accordingly, MAT-MSCs CM experiments paralleled the results of coculture assays (Fig. 5c). These results suggest that MAT-MSCs are involved in the promotion of MCF7 cell EMT process in a TH-dependent manner since the thy-

roid status of breast cancer cells is important to prompt their mesenchymal conversion to facilitate the migration and invasion.

3.5 TH Status of Breast Cancer Cells Influences the Immunomodulatory Properties of MAT-MSCs

Since MAT-MSCs have emerged for their immunosuppressive properties [37], we assessed how the alteration of *DIO2* in MCF7 breast cancer cells might modulate their functional immunomodulatory properties. MAT-MSCs were cocultured or conditioned with the medium of D2KO and WT MCF7 cells, with matched MAT-MSCs monocultured as control, and then the expression of a plethora of immunomodulatory genes, including IL-1 α , IL-1 β , IL-6, IL-8, CXCR4, BAFF, BAFFR, CCL19, CCL21, SDF1 and VEGFA was evaluated (Fig. 6a). While the CM from WT MCF7 cells efficiently enhanced the expression of the above-mentioned inflammatory genes in comparison to MAT-MSCs alone, both in coculture and CM experiments (Fig. 6b,c), the CM from D2KO MCF7 cells failed to stimulate MAT-MSCs in the expression of these genes. To reinforce the concept that TH acts as a potent endocrine signal driving pro-inflammatory effects, we treated MAT-MSCs with the conditioned medium of D2KO MCF7 cells in presence of physiological T3 concentration in a time-course and observed that T3 treatment significantly rescued the expression of the above-mentioned genes, whose levels were enhanced to almost that of MAT-MSCs conditioned with the medium of MCF7 control cells (**Supplementary Fig. 8a**). As an additional control of TH-dependent immune-induction of MAT-MSCs, we treated these latter with the conditioned medium of MCF7 control cells in presence of rT3 in a time-course and observed that the rT3-mediated D2 inhibition, blocking the T4-to-T3 conversion, paralleled the results of MAT-MSCs conditioned with the medium of D2KO MCF7 cells (**Supplementary Fig. 8b**), as indicated by the reduced levels of all the immunomodulatory genes.

In addition, we profiled a panel of cytokines and chemokines released in the CM of D2KO and WT MCF7 cells. Notably, we found a drastic reduction in the secretory profile of D2KO MCF7 cells compared to WT MCF7 cells (Table 1 and **Supplementary Fig. 8c**). Indeed, D2KO MCF7 cells secreted a lower amount of pro-inflammatory cytokines such as IL-1 β , IL-6, IL-8, IL-10 and, conversely a significantly higher amount of anti-inflammatory antagonists such as IL-1RA and IL-6 R alpha (Table 1 and **Supplementary Fig. 8c**). Together, this evidence poses the TH to act as a pro-inflammatory mediator involved in the immune induction of MAT-MSCs.

3.6 In Vivo, Mammary Model of Intraductal Carcinoma Reveals Resistance to Progression Towards Invasiveness in the Absence of Thyroid Hormone Stimuli

To shed light on the TH influence on the early-stage BRCA malignancy, we used a surgery-free intraductal de-

livery model, namely the Mouse-INtraDuctal (MIND) injection, as a tool for *in vivo* characterization of tumor formation and progression. D2KO and WT MCF7 cells (2.0×10^5 cells in 10.0 μ L) were intraductal injected into the fourth abdominal mammary gland of male C57BL/6 mice and cells were allowed to naturally grow (Fig. 7a). Mammary glands were collected 8 weeks post-tumor cell injection, before the development of overt lesions as assessed by palpation, but concurrently with microlesions as confirmed by histological assessment. Hematoxylin/Eosin (H/E) staining showed that both intraductal injections of D2KO and WT MCF7 cells resulted in the formation of solid tumors with necrotic cores, with no evidence of tumor cell leakage into the adjacent adipose tissue (Fig. 7b). Specifically, both D2KO and WT MCF7 MIND tumors were not characterized by an infiltrating fat phenotype but showed a histological profile more comparable to human breast cancers. To confirm whether these tumors were MCF7-derived *in situ* lesions, we tested them for the expression of E-Cadherin and Vimentin markers by immunofluorescence staining. As shown in Fig. 7c, D2KO and WT MCF7 MIND cells, when xenografted to the mouse milk ducts, recapitulated own *in vitro* EMT features. Differently from WT MCF7-derived *in situ* MIND, D2KO MCF7-derived *in situ* MIND was characterized by higher expression of the epithelial marker E-Cadherin and a reduced expression of the mesenchymal marker Vimentin. Thus, the *in vivo* MIND model confirmed what was observed in *in vitro* data, that *DIO2* depletion and the concurrent T4-to-T3 reduction represent a crucial barrier to counteract breast progression toward invasiveness and metastasis.

To keep track of the expansion of breast cancer to distant sites after intraductal engraftment, we processed the peripheral blood of D2KO and WT MCF7-MIND mice in order to detect and separate the fraction of cells sloughing off the main tumor and extravasing into the blood, namely the Circulating Tumor Cells (CTCs). After collecting blood samples, the expression of four specific markers, i.e. Krt8, Krt18, Krt19, and c-Met, whose transcriptomic levels are a typical signature of BRCA progression in the blood of early breast cancer patients [38,39], was analyzed. Interestingly, the above-mentioned breast cancer-related markers were expressed at higher levels in WT MCF7-MIND mice than D2KO MCF7-MIND mice (Fig. 7d).

In conclusion, these data, not only provide new insights into the complex role of TH in tumor biology but represent evidence that TH critically regulates BRCA progression and its dialogue with the surrounding milieu. Consequently, interfering with the TH signal might be a valid strategy for anti-cancer therapies.

4. Discussion

In this study, we report a paracrine effect of Thyroid Hormone in BRCA, reducing tumor growth while pro-

Table 1. Cytokine and chemokine (pg/mL) in Conditioned Media (CM) from monocultured D2KO and WT MCF7 cells.

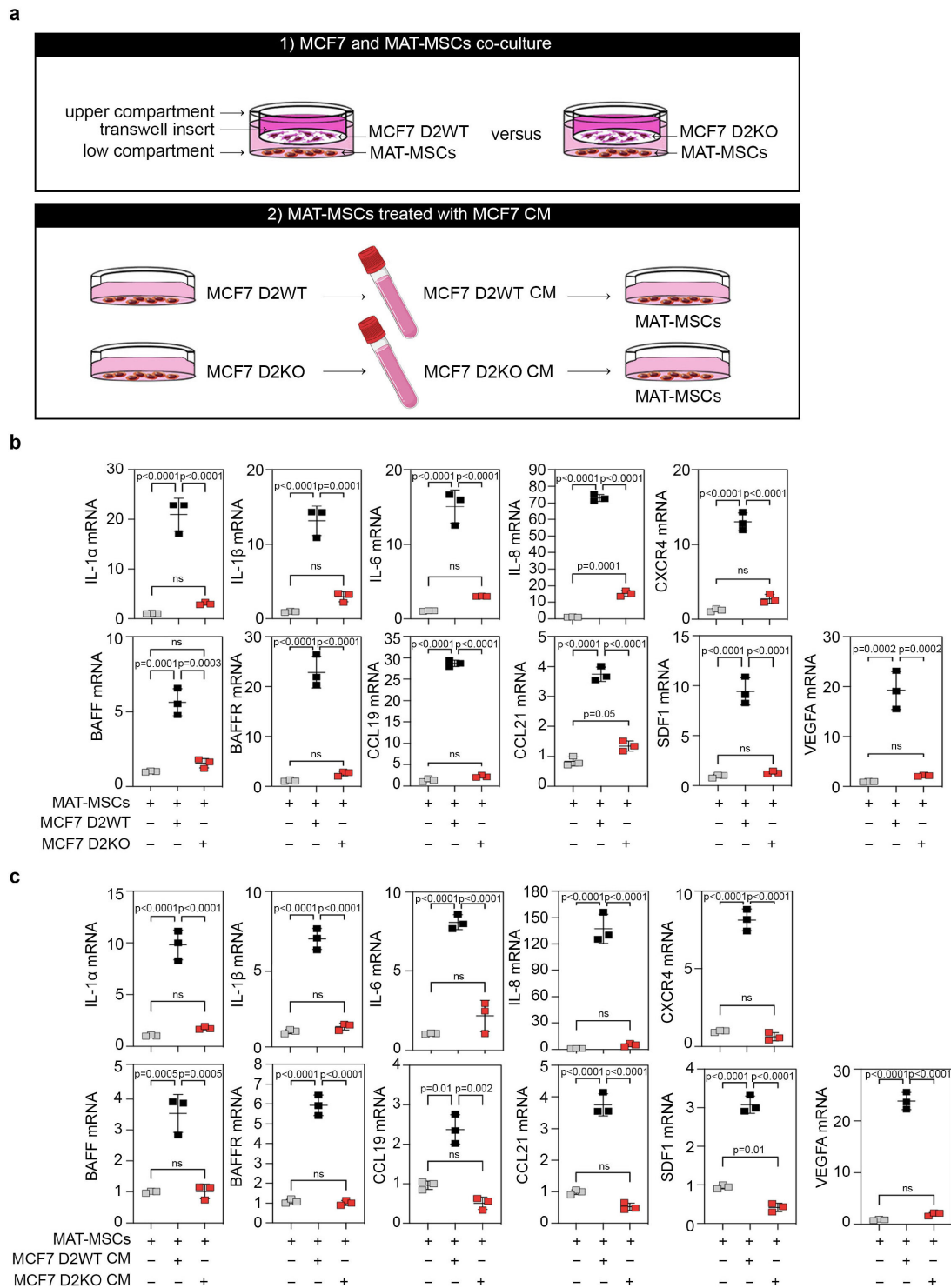
Secreted Factor	MCF7 D2WT CM (pg/mL)	MCF7 D2KO CM (pg/mL)	Statistical Significance	
IL-1 β	7.8 \pm 2.2	4.6 \pm 1.2	<i>t</i> -test	<i>p</i> -value = ns
			One-Sample Wilcoxon Test	<i>p</i> -value = 0.02 vs 0.02
IL-6	2.5 \pm 0.2	1.3 \pm 0.3	<i>t</i> -test	<i>p</i> -value = 0.008
			One-Sample Wilcoxon Test	<i>p</i> -value = 0.002 vs 0.02
IL-8	3453.0 \pm 832.6	2655.9 \pm 1006.3	<i>t</i> -test	<i>p</i> -value = ns
			One-Sample Wilcoxon Test	<i>p</i> -value = 0.02 vs 0.04
IL-10	6.7 \pm 3.7	3.4 \pm 0.9	<i>t</i> -test	<i>p</i> -value = ns
			One-Sample Wilcoxon Test	<i>p</i> -value = ns vs 0.02
IL-1RA	70.1 \pm 7.3	158.6 \pm 35.6	<i>t</i> -test	<i>p</i> -value = 0.01
			One-Sample Wilcoxon Test	<i>p</i> -value = 0.004 vs 0.02
IL-6 R alpha	328.0 \pm 57.2	1125.6 \pm 379.8	<i>t</i> -test	<i>p</i> -value = 0.02
			One-Sample Wilcoxon Test	<i>p</i> -value = 0.01 vs 0.04
BAFF	25.6 \pm 10.9	11.3 \pm 1.2	<i>t</i> -test	<i>p</i> -value = ns
			One-Sample Wilcoxon Test	<i>p</i> -value = 0.05 vs 0.003
VEGF	5006.4 \pm 1149.1	4543.5 \pm 1333.9	<i>t</i> -test	<i>p</i> -value = ns
			One-Sample Wilcoxon Test	<i>p</i> -value = 0.02 vs 0.03
CCL-3	92.3 \pm 14.9	74.2 \pm 2.8	<i>t</i> -test	<i>p</i> -value = ns
			One-Sample Wilcoxon Test	<i>p</i> -value = 0.008 vs 0.0005
CCL-4	137.1 \pm 13.7	113.3 \pm 6.1	<i>t</i> -test	<i>p</i> -value = 0.05
			One-Sample Wilcoxon Test	<i>p</i> -value = 0.003 vs 0.001
CCL-11	150.3 \pm 13.3	119.6 \pm 14.4	<i>t</i> -test	<i>p</i> -value = 0.05
			One-Sample Wilcoxon Test	<i>p</i> -value = 0.003 vs 0.005
CXCL-10	19.4 \pm 4.9	10.2 \pm 2.6	<i>t</i> -test	<i>p</i> -value = 0.04
			One-Sample Wilcoxon Test	<i>p</i> -value = 0.02 vs 0.02
FURIN	2714.7 \pm 894.0	2701.4 \pm 754.5	<i>t</i> -test	<i>p</i> -value = ns
			One-Sample Wilcoxon Test	<i>p</i> -value = 0.03 vs 0.02
CRIPTO	33.2 \pm 18.9	25.2 \pm 10.0	<i>t</i> -test	<i>p</i> -value = ns
			One-Sample Wilcoxon Test	<i>p</i> -value = ns vs 0.05
alpha Synuclein	77.2 \pm 14.2	61.6 \pm 2.4	<i>t</i> -test	<i>p</i> -value = ns
			One-Sample Wilcoxon Test	<i>p</i> -value = 0.01 vs 0.0005
u-PA	194.7 \pm 56.2	138.3 \pm 16.3	<i>t</i> -test	<i>p</i> -value = ns
			One-Sample Wilcoxon Test	<i>p</i> -value = 0.03 vs 0.005
IFN-gamma	27.4 \pm 8.6	18.9 \pm 2.8	<i>t</i> -test	<i>p</i> -value = ns
			One-Sample Wilcoxon Test	<i>p</i> -value = 0.03 vs 0.007
TNF-alpha	7.7 \pm 0.6	22.5 \pm 1.6	<i>t</i> -test	<i>p</i> -value = 0.0001
			One-Sample Wilcoxon Test	<i>p</i> -value = 0.002 vs 0.002
Total Inhibin	126.6 \pm 10.5	92.6 \pm 2.8	<i>t</i> -test	<i>p</i> -value = ns
			One-Sample Wilcoxon Test	<i>p</i> -value = 0.0023 vs 0.0003
APRIL	133.3 \pm 51.3	93.9 \pm 18.6	<i>t</i> -test	<i>p</i> -value = ns
			One-Sample Wilcoxon Test	<i>p</i> -value = 0.05 vs 0.01

72 hours post-plating, CM was collected and analyzed by using the Bio-Plex Multiplex Human Cytokine factor kits (see Methods).

ns, not significant. IL, Interleukin; CCL, C-C motif chemokine ligand.

moting progression, inflammation, and metastasis. These data are in line with the previously demonstrated effects of THs in non-melanoma skin cancer and in prostate cancer [40,41], but importantly, describe a yet unknown role of THs in modulating the crosstalk between MCF7 and the MSCs in breast cancer. According to the classical model of bidirectional crosstalk, the MCF7-produced D2 induces the TH activation, the latter not only regulates the MCF7 endogenous features, but also accelerates MSCs tumori-

genic potential and in turn the MSCs potentiate the invasiveness of MCF7. Thus, our data suggest a potential role played by the intracellular activation of T4 mediated by D2 in breast cancer cells inducing phenotypic and genotypic changes in MSCs *via* a paracrine effect. The discovery that the breast cancer-produced T3 augments the MSCs-dependent invasiveness of tumorigenesis is important and strongly poses T3 as a critical diffuse molecule influencing the tumor stroma crosstalk.



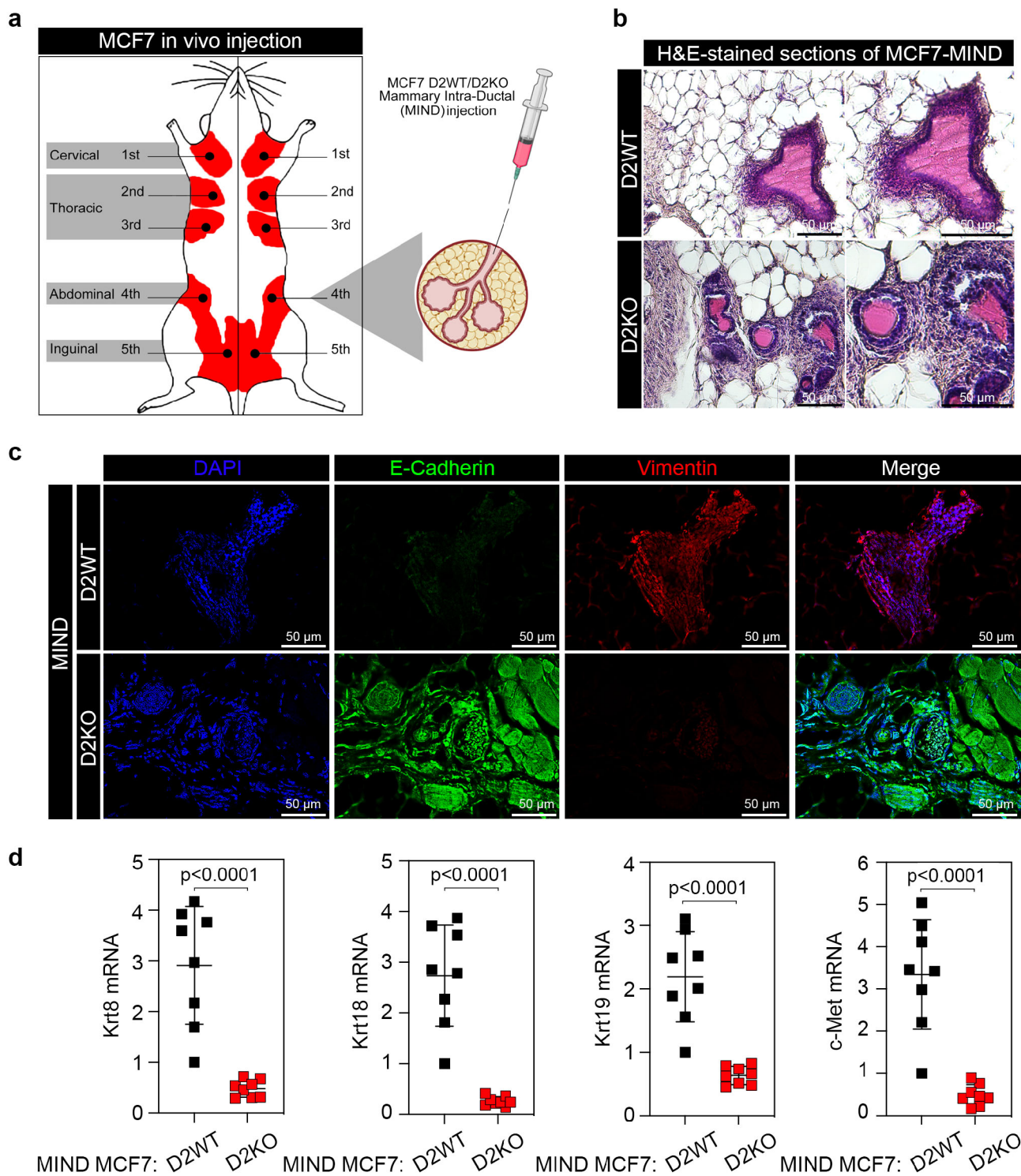


Fig. 7. In vivo characterization of THs-dependent BRCA tumor formation and progression. (a) Schematic representation of Mouse-INtraDuctal (MIND) injection. The experimental protocol is depicted in the panel. (b,c) Hematoxylin/Eosin (H/E) (b) and immunofluorescent staining with epithelial (E-Cadherin) and mesenchymal (Vimentin) markers (c) of D2KO and WT MCF7 MIND tumors (representative of 3 images per sample, $n = 6$ mice/group). Magnification $20\times$. Scale bars represent $50\ \mu\text{m}$. (d) mRNA expression of four metastatic biomarkers (Krt8, Krt18, Krt19 and c-Met) was measured by real-time PCR in circulating tumor cells isolated from blood samples of D2KO and WT MCF7 xenografted MIND mice ($n = 8$ mice/group). All the results are shown as means \pm SD from at least 3 separate experiments. p -values were determined by the two-tailed Student's t -test. Source data are provided as a **Supplementary Source Data file**.

4.1 D2 and Breast Cancer

Although different data in literature have described that the TH-activating enzyme, D2, is up-regulated in advanced human cancers, still few data are available on the expression of D2 in BRCA, and its association with the clinicopathological characteristics of this tumor. By performing a wide *in silico* analysis of different datasets, we described a potent correlation of high *DIO2* expression with poor survival rate for the patients. These data suggest that D2 plays a significant role in aggressive tumors and in the promotion of metastatic potential in BRCA. Moreover, they indicate D2 as a potential useful prognostic marker for patients. Our *in vitro* and *in vivo* experiments confirm the *in silico* data, indicating that D2 inactivation in MCF7 cells drastically attenuates their EMT potential while boosting cell proliferation. The central role of TH in boosting MCF7 invasiveness was further proved by the rescued invasive phenotype of D2KO MCF7 cells treated with T3, as well as by the drastically reduced expression of EMT marker genes induced by treatment of WT MCF7 cells with rT3. Noteworthy, the *in vivo* experiments, based on the intraductal injection of D2KO and WT MCF7 cells, reinforced such a role for D2, since lesions formed by injection of D2KO cells were characterized by an epithelial phenotype, while EMT genes were drastically down-modulated in comparison with lesions formed by the injected WT MCF7 cells.

4.2 The Effects of Thyroid Hormone in the Tumor Microenvironment

In BRCA, chemotactic factors released by cancer cells, which include matrix metalloproteinases, growth factors, and inflammatory cytokines, attract MSCs to the site of tumorigenesis [42]. Furthermore, various tumors, BRCA included, are stimulated by MSCs to grow and progress [43]. In the BRCA context, endogenous MSCs exert powerful pro-tumorigenic activities within the tumor stroma enhancing fibrovascular desmoplasia, tumor growth and metastasis [44,45]. In detail, breast cancer cells stimulate the MSC to secrete different chemokines thereby accelerating the conversion of cancer cells toward invasion and malignancy. Although the stimulation of MSCs has been investigated, the molecules regulating the mechanism by which they crosstalk with the tumor cells have yet been poorly elucidated. Here, we observed that a functional TH activation mediated by D2 is strictly required not only for the intrinsic cancer biology properties of MCF7 cells, but also for their sensitivity to the MSCs-mediated pro-invasive conversion. Noteworthy, our previous works have indicated that the Deiodinases-mediated regulation of T3 availability deeply impacts cancer formation and progression with dynamic and opposite effect on tumor formation and invasion. Indeed, while the D3-mediated THs inactivation occurs in the early phases of tumorigenesis and in the amplification phase of Cancer Stem Cells (CSCs) [46–48], the subsequent D3 down-regulation and D2 up-

regulation enhance the intracellular activation of T4-to-T3 and thus boosts tumor invasiveness and metastatic conversion [15,27,49]. In the light of these evidence, the observed opposite effects of D2 inactivation on MCF7 proliferation and EMT can be ascribed to the ability of THs to reduce cell proliferation while promoting tumor progression. Differently from the above studies, the present work addresses the intricate role of THs in the Tumor Micro-Environment (TME) and in the interplay of cancer cells with the surrounding milieu. Interestingly, we observed that D2 is produced by MCF7 and catalyzes the T4-to-T3 conversion within cancer cells. This in turn amplifies the ability of MSCs to stimulate MCF7 cells and also enhances the sensitivity of MCF7 cells to MSCs conditioning. Blocking D2 interferes with such a dialogue and is thus a valid tool to counteract the crosstalk within the TME.

4.3 The D2-Dependent Thyroid Hormone Activation Enhances the Production of Pro-Inflammatory Cytokines

Malignant evolution of tumors is often triggered by a strong inflammatory response, in which the TME plays a critical role in fostering EMT of cancer cells and secreting a variety of pro-tumorigenic cytokines. While it is generally acknowledged that increased THs are important modulators of inflammation and immune activities [50], still controversial functions have been described on the role of THs in inflammation, probably due to the pleiotropic properties of these hormones and their context-dependent differential effects. Moreover, even less is known about the role of THs as diffusible molecules in the inflammatory properties of the TME. Importantly, we observed that the MSCs-dependent production of a plethora of pro-inflammatory genes, exacerbated by the MCF7-MSCs interplay, was drastically reduced when D2 was inhibited in MCF7 cells. Indeed, our data show that MSCs cultured with MCF7 amplified the inflammatory gene expression, but such effect was lost when MSCs were cultured with D2KO MCF7, and this impairment was completely rescued by the addition of exogenous T3 to the co-cultures.

In conclusion, the current work adds different novel insights into the complex role of THs and its intracellular activation in BRCA. All the data point to a potent effect of THs in exacerbating the tumor invasiveness. These observations are in line with clinical data showing that BRCA is increased in hyperthyroidism [51,52], and that stage I ER⁺ BRCA patients treated with THs for the management of hypothyroidism have worse outcomes [53]. Furthermore, it has been also shown that, acting *via* non-genomic mode, THs foster BRCA formation and invasion [54,55]. In light of the above considerations, we conclude that the intratumoral-activated TH can increase the aggressiveness of BRCA and that the inhibition of the D2 enzyme can be viewed as a valid tool to attenuate BRCA progression. Moreover, our data strengthen the concept that elevated THs levels in hyperthyroid patients can worsen the cancer

risk, suggesting that treatment with THs in patients with both hypothyroidism and BRCA should be finely monitored to ascertain the THs levels in the physiological range.

5. Conclusions

In conclusion, we demonstrated that, according to the classical model of bidirectional crosstalk, the MCF7-produced D2 induces the TH activation. The D2-activated T3 not only regulates the MCF7 endogenous features, but also accelerates MSCs tumorigenic potential, that in turn potentiates the invasiveness of MCF7. Thus, our data suggest a potential role played by the intracellular activation of T4 mediated by D2 in breast cancer cells inducing phenotypic and genotypic changes in MSCs via a paracrine effect. The discovery that the breast cancer-produced T3 augments the MSCs-dependent invasiveness of tumorigenesis is important and strongly poses T3 as a critical diffuse molecule influencing the tumor stroma crosstalk.

Availability of Data and Materials

The data that support the findings of this study are available from the corresponding author upon request.

Author Contributions

AN, VDE, CM, AP, AGC, SS, LA, ST, FR, MR, MM and EDC performed *in vitro* and *in vivo* experiments. AN performed the immunofluorescence and bioinformatic analysis, analyzed the results and provided scientific interpretations. MR performed the FACS analysis studies. PF and MD designed the overall study, supervised the experiments, and analyzed the results. AN, PF and MD wrote the paper. All authors discussed the results and provided input on the manuscript. All authors contributed to editorial changes in the manuscript. All authors read and approved the final manuscript. All authors have participated sufficiently in the work and agreed to be accountable for all aspects of the work.

Ethics Approval and Consent to Participate

All animal procedures were approved by the Institutional Animal Care and Use Committee (IACUC, nos. 167/2015-PR and 354/2019-PR) and conducted in accordance with the guidelines of the “Department of Human Health, Animal Health and Ecosystem and International Relations” from Ministero della Salute (MSAL). The study involving human participants was granted ethical approval by the Surgery Department of the University Hospital Center “Federico II” of Naples, in accordance with Protocol Number 138/16. A written informed consent was obtained from the patients or their families/legal guardians. The study was carried out in compliance with the guidelines of the Declaration of Helsinki.

Acknowledgment

We would like to express our gratitude to all those who helped during the preparation of this manuscript.

Funding

This work was supported by grants awarded to M.D. from AIRC Foundation for Cancer Research in Italy (IG 29242) and Ministero dell’Istruzione, dell’Università e della Ricerca – MIUR (PRIN-2022 Grant, Project Code 2022HB54P9), a grant awarded to P.F. from AIRC Foundation for Cancer Research in Italy (IG 29378) and a grant awarded from MIUR to A.G.C. (PRIN-2022 Grant, Project Code 20223ZWCH2). A.N. was supported by an AIRC Fellowship for Italy Grant (Project Code 26823). C.M. was supported by Fondazione Umberto Veronesi (Project Code 5309).

Conflict of Interest

The authors declare no conflict of interest.

Supplementary Material

Supplementary material associated with this article can be found, in the online version, at <https://doi.org/10.31083/FBL26113>.

References

- [1] Harbeck N, Penault-Llorca F, Cortes J, Gnant M, Housami N, Poortmans P, *et al.* Breast cancer. Nature Reviews. Disease Primers. 2019; 5: 66. <https://doi.org/10.1038/s41572-019-0111-2>.
- [2] Huen MSY, Sy SMH, Chen J. BRCA1 and its toolbox for the maintenance of genome integrity. Nature Reviews. Molecular Cell Biology. 2010; 11: 138–148. <https://doi.org/10.1038/nrm2831>.
- [3] Kuchenbaecker KB, Hopper JL, Barnes DR, Phillips KA, Mooij TM, Roos-Blom MJ, *et al.* Risks of Breast, Ovarian, and Contralateral Breast Cancer for BRCA1 and BRCA2 Mutation Carriers. JAMA. 2017; 317: 2402–2416. <https://doi.org/10.1001/jama.2017.7112>.
- [4] Krishnamurti U, Silverman JF. HER2 in breast cancer: a review and update. Advances in Anatomic Pathology. 2014; 21: 100–107. <https://doi.org/10.1097/PAP.000000000000015>.
- [5] Li CI, Malone KE, Daling JR. Differences in breast cancer hormone receptor status and histology by race and ethnicity among women 50 years of age and older. Cancer Epidemiology, Biomarkers & Prevention: a Publication of the American Association for Cancer Research, Cosponsored by the American Society of Preventive Oncology. 2002; 11: 601–607.
- [6] Margenthaler JA, Ollila DW. Breast Conservation Therapy Versus Mastectomy: Shared Decision-Making Strategies and Overcoming Decisional Conflicts in Your Patients. Annals of Surgical Oncology. 2016; 23: 3133–3137. <https://doi.org/10.1245/s10434-016-5369-y>.
- [7] Davis PJ, Goglia F, Leonard JL. Nongenomic actions of thyroid hormone. Nature Reviews. Endocrinology. 2016; 12: 111–121. <https://doi.org/10.1038/nrendo.2015.205>.
- [8] Davis PJ, Mousa SA, Lin HY. Nongenomic Actions of Thyroid Hormone: The Integrin Component. Physiological Reviews. 2021; 101: 319–352. <https://doi.org/10.1152/physrev.00038.2019>.

- [9] Hercbergs A, Lin HY, Mousa SA, Davis PJ. (Thyroid) Hormonal regulation of breast cancer cells. *Frontiers in Endocrinology*. 2023; 13: 1109555. <https://doi.org/10.3389/fendo.2022.1109555>.
- [10] Tang HY, Lin HY, Zhang S, Davis FB, Davis PJ. Thyroid hormone causes mitogen-activated protein kinase-dependent phosphorylation of the nuclear estrogen receptor. *Endocrinology*. 2004; 145: 3265–3272. <https://doi.org/10.1210/en.2004-0308>.
- [11] Tran TVT, Kitahara CM, Leenhardt L, de Vathaire F, Boutron-Ruault MC, Journy N. The effect of thyroid dysfunction on breast cancer risk: an updated meta-analysis. *Endocrine-related Cancer*. 2022; 30: e220155. <https://doi.org/10.1530/ERC-22-0155>.
- [12] Luongo C, Dentice M, Salvatore D. Deiodinases and their intricate role in thyroid hormone homeostasis. *Nature Reviews. Endocrinology*. 2019; 15: 479–488. <https://doi.org/10.1038/s41574-019-0218-2>.
- [13] Hönes GS, Rakov H, Logan J, Liao XH, Werbenko E, Pollard AS, et al. Noncanonical thyroid hormone signaling mediates cardiometabolic effects in vivo. *Proceedings of the National Academy of Sciences of the United States of America*. 2017; 114: E11323–E11332. <https://doi.org/10.1073/pnas.1706801115>.
- [14] Nappi A, Murolo M, Cicatiello AG, Sagliocchi S, Di Cicco E, Raia M, et al. Thyroid Hormone Receptor Isoforms Alpha and Beta Play Convergent Roles in Muscle Physiology and Metabolic Regulation. *Metabolites*. 2022; 12: 405. <https://doi.org/10.3390/metabo12050405>.
- [15] Cheng SY, Leonard JL, Davis PJ. Molecular aspects of thyroid hormone actions. *Endocrine Reviews*. 2010; 31: 139–170. <https://doi.org/10.1210/er.2009-0007>.
- [16] Brent GA. Mechanisms of thyroid hormone action. *The Journal of Clinical Investigation*. 2012; 122: 3035–3043. <https://doi.org/10.1172/JCI60047>.
- [17] Bassett JH, Harvey CB, Williams GR. Mechanisms of thyroid hormone receptor-specific nuclear and extra nuclear actions. *Molecular and Cellular Endocrinology*. 2003; 213: 1–11. <https://doi.org/10.1016/j.mce.2003.10.033>.
- [18] Schulz M, Salamero-Boix A, Niesel K, Alekseeva T, Sevensen L. Microenvironmental Regulation of Tumor Progression and Therapeutic Response in Brain Metastasis. *Frontiers in Immunology*. 2019; 10: 1713. <https://doi.org/10.3389/fimmu.2019.01713>.
- [19] Hanahan D, Coussens LM. Accessories to the crime: functions of cells recruited to the tumor microenvironment. *Cancer Cell*. 2012; 21: 309–322. <https://doi.org/10.1016/j.ccr.2012.02.022>.
- [20] Lapeire L, Hendrix A, Lambein K, Van Bockstal M, Braems G, Van Den Broecke R, et al. Cancer-associated adipose tissue promotes breast cancer progression by paracrine oncostatin M and Jak/STAT3 signaling. *Cancer Research*. 2014; 74: 6806–6819. <https://doi.org/10.1158/0008-5472.CAN-14-0160>.
- [21] La Camera G, Gelsomino L, Malivindi R, Barone I, Panza S, De Rose D, et al. Adipocyte-derived extracellular vesicles promote breast cancer cell malignancy through HIF-1 α activity. *Cancer Letters*. 2021; 521: 155–168. <https://doi.org/10.1016/j.canlet.2021.08.021>.
- [22] D'Esposito V, Lecce M, Marenzi G, Cabaro S, Ambrosio MR, Sammartino G, et al. Platelet-rich plasma counteracts detrimental effect of high-glucose concentrations on mesenchymal stem cells from Bichat fat pad. *Journal of Tissue Engineering and Regenerative Medicine*. 2020; 14: 701–713. <https://doi.org/10.1002/term.3032>.
- [23] Fang J, Chen F, Liu D, Gu F, Wang Y. Adipose tissue-derived stem cells in breast reconstruction: a brief review on biology and translation. *Stem Cell Research & Therapy*. 2021; 12: 8. <https://doi.org/10.1186/s13287-020-01955-6>.
- [24] Pärth G, Perakakis N, Mantzoros CS, Seufert J. Stem cells in the treatment of diabetes mellitus - Focus on mesenchymal stem cells. *Metabolism: Clinical and Experimental*. 2019; 90: 1–15. <https://doi.org/10.1016/j.metabol.2018.10.005>.
- [25] Kamat P, Schweizer R, Kaenel P, Salemi S, Calcagni M, Giovanoli P, et al. Human Adipose-Derived Mesenchymal Stromal Cells May Promote Breast Cancer Progression and Metastatic Spread. *Plastic and Reconstructive Surgery*. 2015; 136: 76–84. <https://doi.org/10.1097/PRS.0000000000001321>.
- [26] Plava J, Cihova M, Burikova M, Bohac M, Adamkov M, Drachosova S, et al. Permanent Pro-Tumorigenic Shift in Adipose Tissue-Derived Mesenchymal Stromal Cells Induced by Breast Malignancy. *Cells*. 2020; 9: 480. <https://doi.org/10.3390/cell9020480>.
- [27] Kilbas PO, Can ND, Kizilboga T, Ezberci F, Doganay HL, Arisan ED, et al. CRISPR/Cas9-mediated Bag-1 knockout increased mesenchymal characteristics of MCF-7 cells via Akt hyperactivation-mediated actin cytoskeleton remodeling. *PLoS One*. 2022; 17: e0261062. <https://doi.org/10.1371/journal.pone.0261062>. The isolation and Analysis of CTCs from Mice Blood
- [28] Miro C, Nappi A, Sagliocchi S, Di Cicco E, Murolo M, Torabinejad S, et al. Thyroid Hormone Regulates the Lipid Content of Muscle Fibers, Thus Affecting Physical Exercise Performance. *International Journal of Molecular Sciences*. 2023; 24: 12074. <https://doi.org/10.3390/ijms241512074>.
- [29] Sagliocchi S, Murolo M, Cicatiello AG, Miro C, Nappi A, Di Cicco E, et al. Repositioning of Cefuroxime as novel selective inhibitor of the thyroid hormone activating enzyme type 2 deiodinase. *Pharmacological Research*. 2023; 189: 106685. <https://doi.org/10.1016/j.phrs.2023.106685>.
- [30] D'Esposito V, Ambrosio MR, Liguoro D, Perruolo G, Lecce M, Cabaro S, et al. In severe obesity, subcutaneous adipose tissue cell-derived cytokines are early markers of impaired glucose tolerance and are modulated by quercetin. *International Journal of Obesity* (2005). 2021; 45: 1811–1820. <https://doi.org/10.1038/s41366-021-00850-1>.
- [31] Ambrosio MR, Mosca G, Migliaccio T, Liguoro D, Nele G, Schonauer F, et al. Glucose Enhances Pro-Tumorigenic Functions of Mammary Adipose-Derived Mesenchymal Stromal/Stem Cells on Breast Cancer Cell Lines. *Cancers*. 2022; 14: 5421. <https://doi.org/10.3390/cancers14215421>.
- [32] Vishnoi M, Peddibhotla S, Yin W, T Scamardo A, George GC, Hong DS, et al. The isolation and characterization of CTC subsets related to breast cancer dormancy. *Scientific Reports*. 2015; 5: 17533. <https://doi.org/10.1038/srep17533>.
- [33] Ballock RT, Zhou X, Mink LM, Chen DH, Mita BC, Stewart MC. Expression of cyclin-dependent kinase inhibitors in epiphyseal chondrocytes induced to terminally differentiate with thyroid hormone. *Endocrinology*. 2000; 141: 4552–4557. <https://doi.org/10.1210/endo.141.12.7839>.
- [34] Porlan E, Vidaurre OG, Rodríguez-Peña A. Thyroid hormone receptor-beta (TR beta 1) impairs cell proliferation by the transcriptional inhibition of cyclins D1, E and A2. *Oncogene*. 2008; 27: 2795–2800. <https://doi.org/10.1038/sj.onc.1210936>.
- [35] Nappi A, Murolo M, Sagliocchi S, Miro C, Cicatiello AG, Di Cicco E, et al. Selective Inhibition of Genomic and Non-Genomic Effects of Thyroid Hormone Regulates Muscle Cell Differentiation and Metabolic Behavior. *International Journal of Molecular Sciences*. 2021; 22: 7175. <https://doi.org/10.3390/ijms22137175>.
- [36] Bianco AC, Salvatore D, Gereben B, Berry MJ, Larsen PR. Biochemistry, cellular and molecular biology, and physiological roles of the iodothyronine selenodeiodinases. *Endocrine Reviews*. 2002; 23: 38–89. <https://doi.org/10.1210/edrv.23.1.0455>.
- [37] Li H, Dai H, Li J. Immunomodulatory properties of mesenchy-

- mal stromal/stem cells: The link with metabolism. *Journal of Advanced Research*. 2023; 45: 15–29. <https://doi.org/10.1016/j.jare.2022.05.012>.
- [38] Fina E. Signatures of Breast Cancer Progression in the Blood: What Could Be Learned from Circulating Tumor Cell Transcripts. *Cancers*. 2022; 14: 5668. <https://doi.org/10.3390/cancer14225668>.
- [39] Pang S, Xu S, Wang L, Wu H, Chu Y, Ma X, *et al.* Molecular profiles of single circulating tumor cells from early breast cancer patients with different lymph node statuses. *Thoracic Cancer*. 2023; 14: 156–167. <https://doi.org/10.1111/1759-7714.14728>.
- [40] Miro C, Di Giovanni A, Murolo M, Cicatiello AG, Nappi A, Sagliocchi S, *et al.* Thyroid hormone and androgen signals mutually interplay and enhance inflammation and tumorigenic activation of tumor microenvironment in prostate cancer. *Cancer Letters*. 2022; 532: 215581. <https://doi.org/10.1016/j.canlet.2022.215581>.
- [41] Mancino G, Sibilio A, Luongo C, Di Cicco E, Miro C, Cicatiello AG, *et al.* The Thyroid Hormone Inactivator Enzyme, Type 3 Deiodinase, Is Essential for Coordination of Keratinocyte Growth and Differentiation. *Thyroid: Official Journal of the American Thyroid Association*. 2020; 30: 1066–1078. <https://doi.org/10.1089/thy.2019.0557>.
- [42] Ridge SM, Sullivan FJ, Glynn SA. Mesenchymal stem cells: key players in cancer progression. *Molecular Cancer*. 2017; 16: 31. <https://doi.org/10.1186/s12943-017-0597-8>.
- [43] Maffey A, Storini C, Diceglie C, Martelli C, Sironi L, Calzarossa C, *et al.* Mesenchymal stem cells from tumor microenvironment favour breast cancer stem cell proliferation, cancerogenic and metastatic potential, via ionotropic purinergic signalling. *Scientific Reports*. 2017; 7: 13162. <https://doi.org/10.1038/s41598-017-13460-7>.
- [44] Karnoub AE, Dash AB, Vo AP, Sullivan A, Brooks MW, Bell GW, *et al.* Mesenchymal stem cells within tumour stroma promote breast cancer metastasis. *Nature*. 2007; 449: 557–563. <https://doi.org/10.1038/nature06188>.
- [45] Kidd S, Spaeth E, Dembinski JL, Dietrich M, Watson K, Klopp A, *et al.* Direct evidence of mesenchymal stem cell tropism for tumor and wounding microenvironments using in vivo bioluminescent imaging. *Stem Cells (Dayton, Ohio)*. 2009; 27: 2614–2623. <https://doi.org/10.1002/stem.187>.
- [46] Luongo C, Ambrosio R, Salzano S, Dlugosz AA, Missero C, Dentice M. The sonic hedgehog-induced type 3 deiodinase facilitates tumorigenesis of basal cell carcinoma by reducing Gli2 inactivation. *Endocrinology*. 2014; 155: 2077–2088. <https://doi.org/10.1210/en.2013-2108>.
- [47] Torabinejad S, Miro C, Barone B, Imbimbo C, Crocetto F, Dentice M. The androgen-thyroid hormone crosstalk in prostate cancer and the clinical implications. *European Thyroid Journal*. 2023; 12: e220228. <https://doi.org/10.1530/ETJ-22-0228>.
- [48] Cicatiello AG, Ambrosio R, Dentice M. Thyroid hormone promotes differentiation of colon cancer stem cells. *Molecular and Cellular Endocrinology*. 2017; 459: 84–89. <https://doi.org/10.1016/j.mce.2017.03.017>.
- [49] Miro C, Ambrosio R, De Stefano MA, Di Girolamo D, Di Cicco E, Cicatiello AG, *et al.* The Concerted Action of Type 2 and Type 3 Deiodinases Regulates the Cell Cycle and Survival of Basal Cell Carcinoma Cells. *Thyroid: Official Journal of the American Thyroid Association*. 2017; 27: 567–576. <https://doi.org/10.1089/thy.2016.0532>.
- [50] De Vito P, Incerpi S, Pedersen JZ, Luly P, Davis FB, Davis PJ. Thyroid hormones as modulators of immune activities at the cellular level. *Thyroid: Official Journal of the American Thyroid Association*. 2011; 21: 879–890. <https://doi.org/10.1089/thy.2010.0429>.
- [51] Søgaard M, Farkas DK, Ehrenstein V, Jørgensen JOL, Dekkers OM, Sørensen HT. Hypothyroidism and hyperthyroidism and breast cancer risk: a nationwide cohort study. *European Journal of Endocrinology*. 2016; 174: 409–414. <https://doi.org/10.1530/EJE-15-0989>.
- [52] Khan SR, Chaker L, Ruiter R, Aerts JGJV, Hofman A, Dehghan A, *et al.* Thyroid Function and Cancer Risk: The Rotterdam Study. *The Journal of Clinical Endocrinology and Metabolism*. 2016; 101: 5030–5036. <https://doi.org/10.1210/jc.2016-2104>.
- [53] Wahdan-Alaswad RS, Edgerton SM, Salem H, Kim HM, Tan AC, Finlay-Schultz J, *et al.* Exogenous Thyroid Hormone Is Associated with Shortened Survival and Upregulation of High-Risk Gene Expression Profiles in Steroid Receptor-Positive Breast Cancers. *Clinical Cancer Research: an Official Journal of the American Association for Cancer Research*. 2021; 27: 585–597. <https://doi.org/10.1158/1078-0432.CCR-20-2647>.
- [54] Sloan EK, Pouliot N, Stanley KL, Chia J, Moseley JM, Hards DK, *et al.* Tumor-specific expression of alphavbeta3 integrin promotes spontaneous metastasis of breast cancer to bone. *Breast Cancer Research: BCR*. 2006; 8: R20. <https://doi.org/10.1186/bcr1398>.
- [55] Hercbergs A, Mousa SA, Lin HY, Davis PJ. What is thyroid function in your just-diagnosed cancer patient? *Frontiers in Endocrinology*. 2023; 14: 1109528. <https://doi.org/10.3389/fendo.2023.1109528>.